

Detailed heterogeneous chemistry in an urban plume box model: reversible co-adsorption of O₃, NO₂, and H₂O on soot coated with benzo[a]pyrene

M. Springmann¹, D. A. Knopf², and N. Riemer³

¹Department of Physics and Astronomy, Stony Brook University, Stony Brook, NY, USA

²School of Marine and Atmospheric Sciences, Institute for Terrestrial and Planetary Atmospheres, Stony Brook University, Stony Brook, NY, USA

³Department of Atmospheric Sciences, University of Illinois at Urbana-Champaign, Urbana, IL, USA

Received: 27 March 2009 – Published in Atmos. Chem. Phys. Discuss.: 20 April 2009

Revised: 18 June 2009 – Accepted: 13 September 2009 – Published: 7 October 2009

Abstract. This study assesses in detail the effects of heterogeneous chemistry on the particle surface and gas-phase composition by modeling the reversible co-adsorption of O₃, NO₂, and H₂O on soot coated with benzo[a]pyrene (BaP) for an urban plume scenario over a period of five days. By coupling the Pöschl-Rudich-Ammann (PRA) kinetic framework for aerosols (Pöschl et al., 2007) to a box model version of the gas phase mechanism RADM2, we are able to track individual concentrations of gas-phase and surface species over the course of several days. The flux-based PRA formulation takes into account changes in the uptake kinetics due to changes in the chemical gas-phase and particle surface compositions. This dynamic uptake coefficient approach is employed for the first time in a broader atmospheric context of an urban plume scenario. Our model scenarios include one to three adsorbents and three to five coupled surface reactions. The results show a variation of the O₃ and NO₂ uptake coefficients of more than five orders of magnitude over the course of the simulation time and a decrease in the uptake coefficients in the various scenarios by more than three orders of magnitude within the first six hours. Thereafter, periodic peaks of the uptake coefficients follow the diurnal cycle of gas-phase O₃-NO_x reactions. Physisorption of water vapor reduces the half-life of the coating substance BaP by up to a factor of seven by permanently occupying ~75% of the soot surface. Soot emissions modeled by replenishing reactive surface sites lead to maximum gas-phase O₃ depletions

of 41 ppbv and 7.8 ppbv for an hourly and six-hourly replenishment cycle, respectively. This conceptual study highlights the interdependence of co-adsorbing species and their non-linear gas-phase feedback. It yields further insight into the atmospheric importance of the chemical oxidation of particles and emphasizes the necessity to implement detailed heterogeneous kinetics in future modeling studies.

1 Introduction

Heterogeneous chemistry describes reactions between gas-phase species and condensed matter. In the atmosphere, these heterogeneous reactions can significantly change the composition of aerosol particles and the atmospheric environment. The most prominent example is heterogeneous reactions on polar stratospheric clouds, which are the key processes for the observed strong ozone depletion during polar spring (Crutzen and Arnold, 1986; Molina et al., 1987; Solomon et al., 1992).

In the troposphere, changes in aerosol composition due to heterogeneous reactions can affect the particle's hygroscopicity with subsequent consequences for its radiative properties and its interactions with clouds (e.g. Rudich, 2003; Kanakidou et al., 2005; Rudich et al., 2007). Furthermore, heterogeneous reactions can have significant impact on the chemistry of the troposphere by changing gas-phase concentrations of air pollutants and oxidizing agents (e.g. Dentener et al., 1996; Seisel et al., 2005; Evans and Jacob, 2005; Brown et al., 2006; Karagulian et al., 2006; Knopf et al., 2006, 2007; Cosman et al., 2008; Osthoff et al., 2008).



Correspondence to: D. A. Knopf
(daniel.knopf@stonybrook.edu)

Human health can be affected by heterogeneous reactions leading to changes in the aerosol particle's toxicity and allergic potential (Finlayson-Pitts and Pitts, 1997, 2000; Pöschl, 2002; Franze et al., 2003, 2005; Bernstein et al., 2004).

An ubiquitous aerosol particle type, particularly in urban environments, is soot. Soot particles originate from the incomplete combustion of hydrocarbons, e.g. in combustion engines (Finlayson-Pitts and Pitts, 2000; Bond et al., 2004), and may be coated with polycyclic aromatic hydrocarbons (PAHs) formed by the same processes (Finlayson-Pitts and Pitts, 2000).

Laboratory studies indicated that gas phase species such as ozone (O₃) and nitrogen dioxide (NO₂) can react with soot surfaces (Pöschl, 2005; Nienow and Roberts, 2006; Rudich et al., 2007). Ozonolysis experiments on soot showed rapid initial gas uptake followed by a slower uptake regime during which surface reactions occurred (Smith and Chughtai, 1996; Disselkamp et al., 2000; Pöschl et al., 2001). These surface reactions can produce carboxyl groups that stay on the particle surface and/or volatile species such as CO₂ and H₂O that desorb to the gas phase (Thomas et al., 2001). The same two-step kinetic process, fast initial uptake followed by a slower uptake regime, was found in experiments probing the adsorption and reactivity of NO₂ on soot (Ammann et al., 1998; Kleffmann et al., 1999; Saathoff et al., 2001). Studies also indicated the subsequent formation and desorption of nitrous acid (HONO), which is important for initiating daytime photochemistry by providing a source for the hydroxyl radical (OH) (Ammann et al., 1998; Arens et al., 2001, 2002; Vogel et al., 2003; Aubin and Abbatt, 2007). Water vapor significantly affects the ozonolysis of soot and the NO₂ adsorption on soot surfaces. It delays the loss of surface species during ozonolysis (Pöschl et al., 2001) and may decrease the NO₂ uptake.

The efficiency of heterogeneous reactions is often expressed employing an uptake coefficient (γ) which represents the ratio between the net flux of a gas phase species from the gas phase to the condensed phase and the gas kinetic flux of the same gas phase species colliding with the surface (Danckwerts, 1951; Schwartz and Freiberg, 1981; Schwartz, 1986; Pöschl et al., 2007). Modeling studies often assume constant uptake coefficients to describe heterogeneous reactions (Tie et al., 2001; Bey et al., 2001; Aklilu and Michelangeli, 2004), or employ empirical parameterizations of the uptake coefficient in dependence of relative humidity, temperature, and aerosol composition (Evans and Jacob, 2005; Davis et al., 2008). However, the experimental studies on the adsorption of gas-phase species on soot mentioned above indicate that the heterogeneous kinetics depend also on particle surface composition and gas-phase concentrations, in addition to the environmental conditions described by temperature and relative humidity. Consequently, changes in gas-phase composition due to reactions within the gas-phase and uptake of gas-phase species by particles can significantly affect the efficiency of the uptake kinetics. For these reasons,

the uptake coefficient can not a priori be treated as a constant value. Instead, one would expect that it generally varies over time due to changes in the particle surface composition and gas-phase concentrations.

Pöschl et al. (2007) developed a kinetic model framework for aerosol surface chemistry and gas-particle interactions which includes flux-based mass balance and rate equations, and a clear separation of mass transport and chemical reactions. This treatment, also termed the Pöschl-Rudich-Ammann (PRA) framework (Pöschl et al., 2007; Ammann and Pöschl, 2007), allows to consider changes in the rate parameters such as the uptake coefficient as a result of changes in particle surface composition and gas-phase concentrations. For the remainder of this manuscript, we refer to this approach as dynamic uptake coefficient approach emphasizing the potential variability of γ . The PRA framework consists of a double-layer surface model which incorporates gas-surface, surface layer, and surface-bulk reactions and allows the addition of unlimited numbers of chemical species and physicochemical processes (Pöschl et al., 2007). It provides an explicit mechanistic description of concentration and time dependencies of the reactive and non-reactive gas uptake and subsequent changes in particle composition. Using this framework, the two-step kinetic process observed in the ozonolysis and NO₂ adsorption experiments can be described by a Langmuir adsorption-desorption equilibrium followed by Langmuir-Hinshelwood type surface reactions (Pöschl et al., 2001; Rudich, 2003; Rudich et al., 2007; Pöschl et al., 2007).

The focus of this paper is to determine how heterogeneous reactions change the aerosol surface composition and affect the gas-phase concentrations of adsorbing pollutants in an urban plume scenario. To investigate this question, the PRA dynamic uptake coefficient approach is coupled to the Second Generation Regional Acid Deposition Model (RADM2) which is a well-established, nonlinear chemical gas-phase mechanism for modeling atmospheric chemistry on a regional scale (Chang et al., 1987; Stockwell et al., 1990) under consideration of diurnal changes in photolysis frequencies and gas-phase emissions. With this coupled model framework, we are able to assess in yet not achieved detail the effects of heterogeneous reactions on particle and atmospheric gas-phase composition for arbitrary time scales. We apply data from several heterogeneous uptake experiments on soot to model the reversible co-adsorption of O₃, NO₂, and water vapor on soot particles coated with the polycyclic aromatic hydrocarbon benzo[a]pyrene (BaP) for an urban plume scenario. These model substances are of high relevance with respect to public health and the environment, as BaP is classified as a "probable human carcinogen" (EPA, 2006a) and the trace gases O₃ and NO₂ are major criteria air pollutants (EPA, 2006b). With these gas-phase species, we define three model scenarios of increasing complexity which are comprised of adsorption and surface reactions of O₃, of O₃ and NO₂, and of O₃, NO₂, and water vapor. Since each

scenario has a different number of co-adsorbing species, we are able to give a detailed account on the influence of co-adsorption on heterogeneous chemistry and the gas phase. Instead of applying a prescribed uptake coefficient, we explicitly resolve the fluxes that determine the uptake coefficient. Therefore, the uptake coefficient is a quantity that is diagnosed from our calculations and is dependent on adsorbent specific parameters like molecular cross section, accommodation coefficient, desorption time, and the adsorbents' gas-phase and surface concentrations and reactions.

The new contributions of this study are the coupling of the PRA framework to gas-phase chemistry and the co-adsorption of multiple gas-phase species with coupled surface reactions. By including the competing effects of O₃, NO₂, and water vapor, the model complexity goes beyond current laboratory experiments, which consider two co-adsorbing gas-phase species at most (e.g. Pöschl et al., 2001). It also places the heterogeneous reactions into a more realistic atmospheric context with atmospheric humidity levels, gas-phase and soot emissions, and diurnal photolysis patterns.

The scope of this paper is conceptual and relies on some simplifications. For example, the maximum adsorbents' surface coverage is limited to one monolayer, which means that diffusion processes through multiple surface layers are not considered in our model framework. This allows us to treat the uptake of gas-phase species according to Langmuir adsorption kinetics. To reduce complexity, we neglect changes in particle composition due to coagulation, dilution, and condensation of semi-volatile gas-phase species. We also expect more trace gases than the three considered here to adsorb onto soot particles under atmospheric conditions. However, with limiting the number of adsorbents to three, we are able to specifically assess each adsorbent's influence on the heterogeneous chemistry. Other trace gases, such as OH and NO₃, are also involved in important heterogeneous reactions (e.g. Bertram et al., 2001; Molina et al., 2004; Hearn and Smith, 2006; Knopf et al., 2006; Gross and Bertram, 2008; Park et al., 2008; Gross and Bertram, 2009), but have not been shown to adhere to Langmuir adsorption kinetics with subsequent surface reactions (Langmuir-Hinshelwood type reactions) and are therefore not the subject of this study. Although we attempt to use realistic values characteristic of an urban plume scenario as input parameters, our purpose is not to make exact atmospheric predictions.

The paper is organized as follows. Section 2 describes the employed model framework consisting of the PRA model framework coupled to the gas-phase solver RADM2. In Sect. 3, we outline our model approach by describing the adapted gas-phase chemistry of an urban plume scenario, the representation of soot coated with BaP as a model substance, our model scenarios with the implemented surface reactions, and additional soot emission scenarios. Section 4 presents our results on the temporal evolution of surface composition, the BaP half-life, and the feedback on the gas-phase O₃

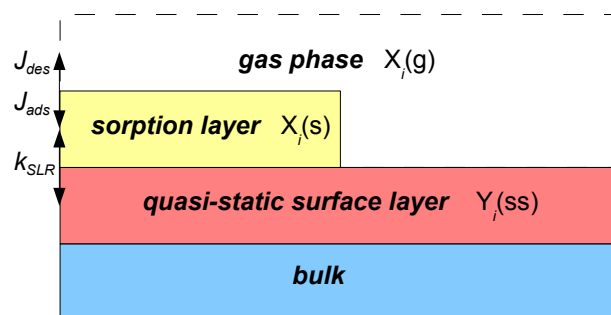


Fig. 1. The applied surface layer model is shown as a schematic. The gas-particle interface is divided into a gas-phase (g) with gas-phase species $X_i(g)$, a sorption layer (s) with adsorbed gas-phase species $X_i(s)$, a quasi-static surface layer (ss) with non-volatile particle components $Y_i(ss)$, and a particle bulk. The adsorption and desorption fluxes are indicated as J_{ads} and J_{des} , respectively, and the rate coefficient for surface layer reactions is denoted by k_{SLR} . Adapted from Pöschl et al. (2007).

concentration for the dynamic uptake approach and, for comparison, for an approach with constant uptake coefficients. We conclude with summarizing the findings and their atmospheric implications.

2 Coupled PRA model framework

The PRA framework (Pöschl et al., 2007) describes gas-phase uptake and surface chemistry by a double-layer surface model with sorption layer and quasi-static layer, and by flux-based rate equations. Figure 1 shows the scenario we adapt on this basis, supported by experiments on the adsorption and subsequent reaction of O₃ on soot (Pöschl et al., 2001) and NO₂ on soot (Ammann et al., 1998): Gas-phase species $X_i(g)$ adsorbs onto the sorption layer, quantified by the adsorption flux J_{ads} . Adsorbed species $X_i(s)$ can then either desorb, expressed by the desorption flux J_{des} , or react with non-volatile particle components $Y_i(ss)$ from the quasi-static surface layer, which is indicated by a second-order rate coefficient k_{SLR} .

The coupling of the PRA model framework to the gas-phase mechanism RADM2 is achieved by implementing the PRA framework's net production and loss terms of gas-phase and surface species into the chemical integration routine of RADM2. Section 2.1 describes the gas-phase loss due to the reversible co-adsorption of gas-phase species using a dynamic uptake approach and Sect. 2.2 gives an account of the chemical production and loss of adsorbed and surface species due to Langmuir-Hinshelwood type surface reactions.

2.1 Dynamic uptake coefficient approach

The presented derivations are relevant to couple the gas-phase mechanism RADM2 to the PRA framework (Pöschl et al., 2007; Ammann and Pöschl, 2007). The subsequent equations represent a condensed version of the PRA framework and follow closely its derivations outlined in Pöschl et al. (2007) and Ammann and Pöschl (2007).

The uptake coefficient of gas species X_i, γ_{X_i}, is defined, in terms of fluxes, as the ratio between the net flux of X_i to the condensed phase, J_{net,X_i}, and the gas kinetic flux of X_i colliding with the surface, J_{coll,X_i}:

$$\gamma_{X_i} = \frac{J_{\text{net},X_i}}{J_{\text{coll},X_i}}. \quad (1)$$

It is important to note that this definition of γ_{X_i} does not explicitly include chemical reactions or gas-phase diffusion, as is often assumed when referring to the reactive uptake coefficient.

The collision flux is based on kinetic gas theory and can be expressed as

$$J_{\text{coll},X_i} = [X_i]_{\text{gs}} \frac{\omega_{X_i}}{4}, \quad (2)$$

where [X_i]_{gs} is the gas-phase concentration close to the surface and ω_{X_i} is the mean thermal velocity of molecule X_i given by ω_{X_i} = √(8RT/(πM_{X_i})), where R is the universal gas constant, T is the absolute temperature, and M_{X_i} is the molar mass of species X_i.

Significant net uptake of the gas-phase species can lead to its local depletion close to the surface. A gas-phase diffusion correction factor C_{g,X_i} can be applied to relate the gas-phase concentration close to the surface [X_i]_{gs} to the average gas-phase concentration [X_i]_g, such that C_{g,X_i} = $\frac{[X_i]_{\text{gs}}}{[X_i]_{\text{g}}}$. For γ_{X_i}-values smaller than one, which is justified for the scenarios considered here, C_{g,X_i} can be determined as (Fuchs and Sutugin, 1971)

$$C_{g,X_i} = \frac{1}{1 + \gamma_{X_i} \frac{0.75 + 0.28 \text{Kn}_{X_i}}{\text{Kn}_{X_i} (1 + \text{Kn}_{X_i})}}, \quad (3)$$

where Kn_{X_i} is the Knudsen number given by

$$\text{Kn}_{X_i} = \frac{6 D_{g,X_i}}{\omega_{X_i} d_p}. \quad (4)$$

D_{g,X_i} is the gas-phase diffusion coefficient of species X_i and d_p is the particle diameter. Using the diffusion coefficients for O₃, NO₂, and water vapor given by Massman (1998) and a particle diameter of 119 nm for soot (Pöschl et al., 2001) results in Knudsen numbers of about 2.17 for NO₂ and H₂O and 2.35 for O₃. Sensitivity runs with and without gas-phase diffusion corrections showed no difference for the case of O₃ and H₂O uptake, and only a difference within the first 10 s of maximum 2% for NO₂ uptake. For this reason, the gas-phase

diffusion correction for the cases considered here can be neglected and the gas-phase concentration close to the surface equals the average gas-phase concentration, [X_i]_{gs} ≈ [X_i]_g.

The net flux to the condensed phase is the difference of the adsorption flux and desorption flux,

$$J_{\text{net},X_i} = J_{\text{ads},X_i} - J_{\text{des},X_i}. \quad (5)$$

The adsorption flux of a gas molecule X_i is related to the collision flux via the accommodation coefficient α_{s,X_i} representing the molecule's probability of adsorption on the surface:

$$\alpha_{s,X_i} = \frac{J_{\text{ads},X_i}}{J_{\text{coll},X_i}}. \quad (6)$$

Thus, J_{ads,X_i} can be expressed as

$$J_{\text{ads},X_i} = \alpha_{s,X_i} J_{\text{coll},X_i} = \alpha_{s,X_i} \frac{\omega_{X_i}}{4} [X_i]_{\text{gs}}. \quad (7)$$

In case of competitive co-adsorption of several gas-phase species, the accommodation coefficient of the individual species, α_{s,X_i}, can be derived using a Langmuir adsorption model in which all adsorbate species compete for a single sorption site on the quasi-static surface, such that

$$\alpha_{s,X_i} = \alpha_{s,0,X_i} (1 - \theta_s), \quad (8)$$

where α_{s,0,X_i} is the surface accommodation coefficient on an adsorbate-free surface. θ_s is the sorption layer surface coverage which is given by the sum of fractional surface coverages of all competing adsorbate species, θ_{s,X_p}, i.e. θ_s = ∑_p θ_{s,X_p}. The fractional surface coverage depends on the surface concentration of the adsorbate species X_p, [X_p]_s, and its effective molecular cross section, σ_{s,X_p}, which corresponds to the inverse of the species' maximum surface concentration in the sorption layer, [X_p]_{s,max}:

$$\theta_{s,X_p} = [X_p]_s / [X_p]_{s,\text{max}} = \sigma_{s,X_p} [X_p]_s. \quad (9)$$

The desorption flux of species X_i can be quantified by the ratio between this species' surface concentration [X_i]_s and its desorption lifetime τ_{d,X_i} which is the mean residence time of the species on the surface:

$$J_{\text{des},X_i} = [X_i]_s / \tau_{d,X_i}. \quad (10)$$

By combining Eqs. (1)–(10) and assuming [X_i]_{gs} = [X_i]_g, the uptake coefficient of species X_i can be derived as

$$\begin{aligned} \gamma_{X_i} &= \frac{J_{\text{ads},X_i} - J_{\text{des},X_i}}{J_{\text{coll},X_i}} \\ &= \frac{\frac{1}{4} \alpha_{s,0,X_i} \omega_{X_i} [X_i]_g (1 - \sum_p \sigma_{s,X_p} [X_p]_s) - \frac{[X_i]_s}{\tau_{d,X_i}}}{\frac{1}{4} \omega_{X_i} [X_i]_g}. \end{aligned} \quad (11)$$

Equation (11) shows that the uptake coefficient derived according to Pöschl et al. (2007) depends on the parameters of the adsorbing species such as α_{s,0,X_i}, σ_{s,X_p}, ω_{X_i}, τ_{d,X_i}, but also on its surface and gas-phase concentrations [X_i]_s and

$[X_i]_g$, which can be affected by transport and chemical reactions. Therefore, Eq. (11) expresses γ_{X_i} as a dynamic uptake coefficient when changes in $[X_i]_s$ and $[X_i]_g$ are taken into account. The numerator of Eq. (11) describes the net flux of $X_i(g)$ to the particle and hence the generation of $X_i(s)$ in the sorption layer under consideration of the surface coverage of all adsorbing species. Surface reactions need to be taken into account to obtain the total net production of sorption layer species, which we outline in Sect. 2.2. It should be noted that the initial adsorbent surface concentration in the sorption layer is zero, thus, the uptake coefficient's initial value is given by the accommodation coefficient, $\gamma_{X_i,ini} = \alpha_{s,0,X_i}$.

The net gas-phase loss of adsorbent X_i , i.e. loss L due to uptake onto the particle in the condensed phase minus production P due to desorption back to the gas phase, is calculated by multiplying the adsorbent's collision flux by the corresponding dynamic uptake coefficient and by the particle surface area in air, $[PS]_g$:

$$\begin{aligned} \left[\frac{d}{dt} [X_i]_g \right]_{\text{uptake}} &= L_{g,p,X_i} - P_{g,p,X_i} = J_{\text{coll},X_i} \gamma_{X_i} [PS]_g \\ &= \gamma_{X_i} [PS]_g [X_i]_g \frac{\omega_{X_i}}{4}. \end{aligned} \quad (12)$$

The next section describes the reaction kinetics between the adsorbed species and surface components according to a Langmuir-Hinshelwood reaction mechanism.

2.2 Langmuir-Hinshelwood mechanism for surface reactions

The Langmuir-Hinshelwood mechanism describes reactions in which adsorbed gas-phase species react on the particle surface (Pöschl et al., 2007). For the cases considered here, we focus on particle surface reactions between the sorption layer (s) and the quasi-static surface layer (ss) following the derivations by Pöschl et al. (2007) and Ammann and Pöschl (2007). Chemical reactions that proceed between the gas phase and the particle surface, exclusively within the sorption or the quasi-static surface layer, as well as photo-chemical processes on the surface are neglected. We assume the product of the surface reactions to be a surface component residing within the quasi-static surface layer. Applying these assumptions, the net chemical production of quasi-static surface species $Y_i(ss)$ from reaction between adsorbed species in the sorption layer, $X_p(s)$, and surface components in the quasi-static surface layer, $Y_q(ss)$, is determined by

$$\begin{aligned} \frac{d}{dt} [Y_i]_{ss} &= P_{s,ss,Y_i} - L_{s,ss,Y_i} \\ &= \sum_v \sum_p \sum_q c_{\text{SLR},v,s,Y_i} k_{\text{SLR},v,X_p,Y_i} [X_p]_s [Y_q]_{ss}, \end{aligned} \quad (13)$$

where v numbers the rate equation, p and q number the reactants, c_{SLR} are negative or positive stoichiometric coefficients, and k_{SLR} are second-order rate coefficients.

In contrast to quasi-static surface layer components which are produced and lost through surface reactions, adsorbed sorption layer species are only depleted by surface reactions, since we assume the surface reactions considered here to be irreversible. The loss of sorption layer species X_i due to the surface reactions is a subset of Eq. (13) with the reactant summation index variable p fixed to species X_i :

$$L_{s,ss,X_i} = \sum_v \sum_q c_{\text{SLR},v,s,X_i} k_{\text{SLR},v,X_i,Y_i} [X_i]_s [Y_q]_{ss}. \quad (14)$$

The total net chemical production of sorption layer species $X_i(s)$ is composed of the loss due to surface reactions and the production and loss due to adsorption and desorption:

$$\frac{d}{dt} [X_i]_s = J_{\text{ads},X_i} - J_{\text{des},X_i} - L_{s,ss,X_i}, \quad (15)$$

where the fluxes of adsorption and desorption, J_{ads,X_i} and J_{des,X_i} , respectively, are described in Sect. 2.1.

The differential Eqs. (12), (13), and (15) represent the heterogeneous kinetics adapted in our model framework. We implement these differential equations into the chemical integration routine of RADM2 (Chang et al., 1987; Stockwell et al., 1990) to obtain solutions and to account for the temporal evolution of the gas phase.

In the next section, we specify the gas-phase chemistry of RADM2 and give a detailed account of our model approach and implemented heterogeneous chemistry scenarios.

3 Model approach

We model the reversible co-adsorption and subsequent surface reactions of O₃, NO₂, and water vapor on soot coated with BaP in an urban plume scenario. Section 3.1 describes the gas-phase chemistry of this urban plume scenario as implemented into the chemical gas-phase solver RADM2. Section 3.2 gives a representation of soot coated with BaP as a model substance, which is followed by an overview of the implemented surface reactions and corresponding model scenarios in Sect. 3.3. Section 3.4 describes two soot emission scenarios to assess the gas-phase feedback from heterogeneous reactions under polluted conditions.

3.1 Gas-phase chemistry

The chemical gas-phase solver RADM2 includes 62 chemical species, 21 photolysis reactions, and 140 thermal reactions (Stockwell et al., 1990). A detailed account of the gas-phase reactions of RADM2 is given elsewhere (Chang et al., 1987; Stockwell et al., 1990). RADM2 is widely used in atmospheric models to predict concentrations of oxidants and other air pollutants (e.g. Grell et al., 2005; Tie et al., 2007). The main feature that RADM2 provides to this study is the NO_x-O₃ chemistry with its diurnal pattern. This results in continuous changes in the O₃ and NO₂ gas-phase concentrations throughout the simulation period. These variations in

gas-phase concentrations subsequently affect the magnitude of the individual and combined uptake of O₃ and NO₂ by the soot particles. This investigation of the gas phase-particle surface interrelationship under atmospherically relevant conditions is one of the main foci and novelty of this study.

We use RADM2 in a tropospheric urban plume scenario (PLUME1) according to Kuhn et al. (1998). This case was designed to represent the chemistry in the polluted boundary layer, which is consistent with an urban plume scenario where emissions of soot occur. This plume scenario includes constant emissions for a variety of trace gases representative for continental European air (Derwent and Jenkin, 1991), such as 0.54 pptv min⁻¹ of SO₂, 2.68 pptv min⁻¹ of NO, and 5.85 pptv min⁻¹ of CO. Volatile organic compounds (VOCs) are aggregated into 15 classes of reactive organic species with emissions of 0.14 pptv min⁻¹ for formaldehyde (HCHO), 0.037 pptv min⁻¹ for acetaldehyde and higher aldehydes, and 0.46 pptv min⁻¹ for acetone, methyl ethyl ketone and higher ketones. Initial concentrations are set to 50 ppbv for O₃, 0.5 ppbv for NO₂, 0.2 ppbv for NO, and 20 000 ppmv for H₂O which corresponds to 64% relative humidity (RH). Time-dependent photolysis rates are calculated as described in Kuhn et al. (1998). Physical processes such as deposition and dilution of trace gases and soot particles, and particle coagulation are not considered. As suggested by Vogel et al. (2003), the reaction rate for the production of HONO from NO and OH was revised according to Atkinson et al. (2001).

RADM2 is run in a box model version for a modeling period of five days, under atmospheric conditions of 1013.25 hPa pressure and a temperature of 298 K. The simulation starts at 12 noon. The gas-phase chemistry in RADM2 is solved with a variable chemical time step (Chang et al., 1987) ranging from 0.096 s to 3 s. To resolve the rapid adsorption of water vapor in scenario C, a shorter time step is used for the first day of the simulation period, ranging from 0.003 s to 0.006 s. The gas-phase solver RADM2 and the heterogeneous chemistry part outlined in the last section run in a coupled fashion for all model scenarios considered in this paper.

3.2 Representation of soot

The chemical surface reactions occur on a population of soot particles coated with BaP. We adopted an initial soot concentration of 10 μg m⁻³ in air corresponding to concentrations in heavily polluted air (Seinfeld and Pandis, 2006). Since the soot surface is of fractal-like geometry (Van Gulijk et al., 2004), we use the surface area obtained from Brunauer-Emmett-Teller (BET) isotherms as reactive surface area and implement a BET value of 500 m² g⁻¹. This corresponds to values that have been used in laboratory heterogeneous chemistry studies (e.g. Tabor et al., 1994; Choi and Leu, 1998; Disselkamp et al., 2000). Multiplying the BET value by the soot concentration yields a total surface concentration

of [PS]_g = 5 × 10⁻⁵ cm² cm⁻³. However, BET values for soot can range from 6 m² g⁻¹ for aircraft engine combustor soot (Popovicheva et al., 2008) to approximately 500 m² g⁻¹ for the post-treated black carbon Degussa FW2 (Dymarska et al., 2006), which can lead to large differences in [PS]_g. Thus, the implemented BET-value of 500 m² g⁻¹ may result in an upper limit for the concentration of surface reaction sites.

While the surface concentration remains constant in this model, the passivation of the surface is introduced by the consumption of the BaP coating, which has initially a surface concentration of 1 × 10¹⁴ cm⁻² corresponding to a full monolayer coverage. BaP readily adsorbs onto soot particles and can be regarded as a proxy for the wider class of polycyclic aromatic compounds, but also for soot due to its structural similarities of the surface (Pöschl et al., 2001). Soot can be pictured as agglomerate of graphene layers, while BaP (C₂₀H₁₂) represents a single graphene layer consisting of five six-membered aromatic rings (Homann, 1998; Pöschl et al., 2001). Here, BaP provides consumable reactive sites for adsorption processes and surface reactions.

3.3 Surface reactions

We define three model scenarios with an increasing level of complexity. These scenarios represent the adsorption and surface reactions of O₃ in scenario A, of O₃ and NO₂ in scenario B, and of O₃, NO₂, and water vapor in scenario C. As starting point for the dynamic uptake coefficient approach described in Sect. 2.1, we implemented experimentally determined initial uptake coefficients as accommodation coefficients in accord to Ammann and Pöschl (2007). This approach is justified, since initially $\gamma_{X_i} = \alpha_{s,0,X_i}$, as can be seen from Eq. (11). In the following, we discuss each scenario with regards to the implemented surface reactions and adapted input parameters with reference to Table 1.

Scenario A represents the adsorption of O₃ and subsequent surface reactions of O₃ with BaP and its derivatives. After O₃ is adsorbed to the sorption layer (s), it participates in three surface reactions with the quasi-static surface layer (ss), (R1) to (R3), as given in Table 1. These reactions convert BaP into chemical derivatives Y2, Y3, and Y4, whose chemical form is not exactly known, but can be pictured as BaP derivatives with an increasing number of oxygenated functional groups and decreasing reactivity towards photo-oxidants such as BaP-quinones, hydroxy-ketones, acid anhydrides, lactones, etc. (Letzel et al., 1999a,b, 2001; Pöschl, 2002). This scenario corresponds to Model System Solid 1 (Ammann and Pöschl, 2007), except that it includes the atmospheric context by the coupling to RADM2. The reaction rate k_{SLR1} and the O₃-specific parameters $\alpha_{s,0,O_3}$, σ_{O_3} , τ_{d,O_3} are adapted from results of aerosol flow tube experiments at ambient temperature and pressure (Pöschl et al., 2001). The reaction rate coefficients for reactions (R2) and (R3), k_{SLR2} and k_{SLR3} , were chosen according to Ammann and Pöschl

(2007) to account for the decreasing reactivity of the BaP derivatives.

Scenario B represents the co-adsorption and subsequent surface reactions of O₃ and NO₂. In addition to surface reactions (R1) to (R3), adsorbed NO₂ also reacts with BaP derivatives according to surface reactions (R4) and (R5) as listed in Table 1. Based on Model System Solid 2 (Ammann and Pöschl, 2007), the products consist of another surface component (with increased oxygenated functional group) and a volatile component which desorbs to the gas-phase. Input parameters are based on experimental data for the reaction and adsorption of NO₂ at the surface of soot particles in Knudsen cell experiments (Gerecke et al., 1998), aerosol flow reactor experiments (Ammann et al., 1998), and filter deposition experiments (Ammann et al., 1997). The reaction rate coefficient for surface reaction (R4), k_{SLR4} , was adjusted by Ammann and Pöschl (2007) to fit the experimental data. In surface reaction (R5), we identify the volatile component with nitrous acid (HONO) and apply a reaction rate of $3.7 \times 10^{-3} \text{ s}^{-1}$ according to Ammann et al. (1998), which yields $7.5 \times 10^{-21} \text{ cm}^2 \text{ s}^{-1}$.

Scenario C involves the co-adsorption of O₃, NO₂, and water vapor, with subsequent surface reactions of O₃ and NO₂ according to surface reactions (R1) to (R5) as listed in Table 1. For this scenario, we assume that water vapor adsorbs to the surface without being involved in subsequent surface reactions. This is supported by Pöschl et al. (2001), who observed a slower decay of BaP and smaller gas-phase O₃ loss under humid conditions indicating the inhibition of O₃ adsorption by competitive adsorption of water vapor at the aerosol surface. Since freshly emitted discharge soot particles are known to be hydrophobic, physisorption of water vapor on soot was suggested as mechanism for adsorption, supported by the water vapor's small desorption lifetime (Pöschl et al., 2001). The H₂O specific parameters $\alpha_{\text{s},\text{O},\text{H}_2\text{O}}$ and $\tau_{\text{d},\text{H}_2\text{O}}$ are adapted from Rogaski et al. (1997) and Pöschl et al. (2001), and $\sigma_{\text{H}_2\text{O}}$ is taken from Nishino (2001).

In our first set of simulations we start with an initial soot concentration and do not include any emissions of fresh soot over the course of the simulation. While the surface concentration $[\text{PS}]_{\text{g}}$ remains constant, the uptake coefficient γ_{X_i} does change with time, according to the available surface reaction sites and gas concentrations, which is explicitly predicted from Eq. (11). In the second set of simulations, we also keep the surface concentration constant, but include the effect of soot emissions by replenishing the reactive surface sites, which we describe in the next section.

3.4 Soot emissions

In polluted areas, soot is emitted continuously by a variety of sources, such as car traffic (Finlayson-Pitts and Pitts, 2000; Bond et al., 2004). Once emitted, the surface of soot particles is expected to become passivated as surface sites are taken up by adsorbents. Therefore, at any given point in time, soot

particles of different ages with different surface reactivities co-exist, ranging from freshly emitted particles with large numbers of reactive surface sites to aged particles where most of the surface sites are depleted. In such an environment, the continuous emission of fresh soot particles could be important when estimating the gas-phase feedback from heterogeneous reactions on soot. In our box model framework, individual soot particles that are introduced at different times due to continuous emissions cannot be tracked. Nevertheless, to estimate the effect of freshly emitted soot particles on the gas phase in our box-model framework, we adopt the following approach as a sensitivity study.

The emission of fresh soot in our box model is approximated by resetting the soot surface to its initial condition with a BaP surface concentration of $[\text{BaP}] = 1 \times 10^{14} \text{ cm}^{-2}$ and no secondary surface components. At this point in the simulation, the existing population of soot with the residual BaP concentration and higher order surface components is discarded. While the number of reactive surface sites changes to account for the effect of soot emissions on chemical reactions, we assume the overall soot production and loss to be in equilibrium and therefore keep the soot surface concentration $[\text{PS}]_{\text{g}}$ constant. We neglect physical processes, such as coagulation, deposition, and dilution of the soot particles. The BaP surface concentration on soot is replenished according to the two following scenarios. In the low emission scenario, the reactive surface is replenished every six hours, and in the high emission scenario, it is replenished every hour. The error from neglecting gas-phase uptake on discarded populations for these replenishing times will be assessed in the next section.

The replenishing times are related to hourly emission rates, R_{emission} , by

$$R_{\text{emission}} = \frac{[\text{PS}]_{\text{g}} \cdot h_{\text{box}}}{\text{BET} \cdot t_{\text{r}}}, \quad (16)$$

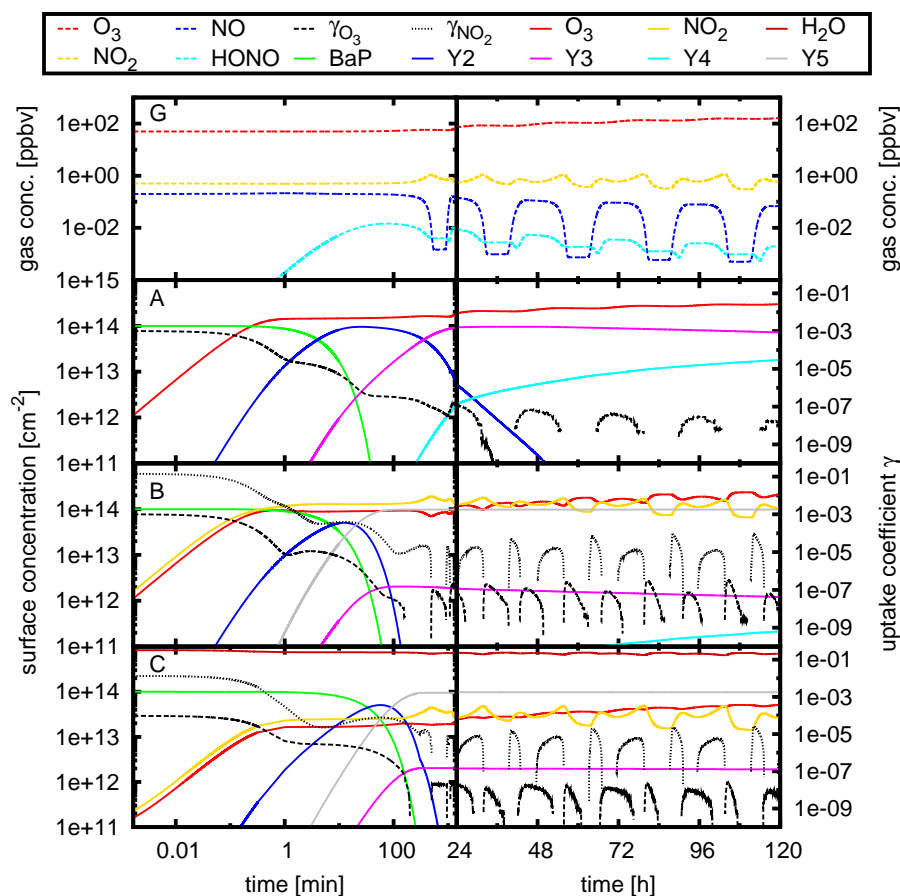
where $[\text{PS}]_{\text{g}} = 5 \times 10^{-5} \text{ cm}^2 \text{ cm}^{-3}$ is the particle surface concentration, $\text{BET} = 500 \text{ m}^2 \text{ g}^{-1}$, t_{r} is the replenishing time, and h_{box} is the box height which we choose as 1 km corresponding to the depth of the tropospheric boundary layer. This yields hourly emission rates of $1.67 \text{ kg km}^{-2} \text{ h}^{-1}$ for the low emission scenario with $t_{\text{r}} = 6 \text{ h}$, and $10 \text{ kg km}^{-2} \text{ h}^{-1}$ for the high emission scenario with $t_{\text{r}} = 1 \text{ h}$. These emission rates are comparable in magnitude to the soot emission rates of $0.72 \text{ kg km}^{-2} \text{ h}^{-1}$ and $7.2 \text{ kg km}^{-2} \text{ h}^{-1}$ chosen in a previous study by Akilu and Michelangeli (2004) to model typical atmospheric background conditions with the lower rate and locations close to urban combustion sources with the higher rate.

This completes our set of model scenarios consisting of the co-adsorption scenarios A, B, and C, and the two classes of emission scenarios which are labeled by the number of replenishments per day as A_{4x} , B_{4x} , C_{4x} , and A_{24x} , B_{24x} , C_{24x} . For matters of comparison, we define additional scenarios at

Table 1. Adsorbents, surface reactions, reaction rates, and parameters – accommodation coefficient (α), effective molecular cross section (σ), desorption time (τ) – applied in model scenarios A, B, C.

Scenario	adsorbents	Surface reactions	Reaction rates [cm ² s ⁻¹]	Parameters
A	O ₃	(R1) O ₃ (s)+BaP(ss)→Y2(ss) (R2) O ₃ (s)+Y2(ss)→Y3(ss) (R3) O ₃ (s)+Y3(ss)→Y4(ss)	$k_{\text{SLR1}}=2.1 \times 10^{-17\text{a,b}}$ $k_{\text{SLR2}}=2.1 \times 10^{-19\text{b}}$ $k_{\text{SLR3}}=2.1 \times 10^{-21\text{b}}$	$\alpha_{\text{s,0,O}_3}=1 \times 10^{-3\text{a,b,c}}$ $\sigma_{\text{O}_3}=1.8 \times 10^{-15} \text{ cm}^{2\text{a,b}}$ $\tau_{\text{d,O}_3}=18 \text{ s}^{\text{a,b}}$
B	O ₃ , NO ₂	(R1) to (R3) (R4) NO ₂ (s)+Y2(ss)→Y5(ss) (R5) NO ₂ (s)+Y3(ss)→HONO(g)	$k_{\text{SLR4}}=7 \times 10^{-18\text{b}}$ $k_{\text{SLR5}}=7.5 \times 10^{-21\text{d,b}}$	$\alpha_{\text{s,0,NO}_2}=0.14^{\text{e,b}}$ $\sigma_{\text{NO}_2}=3 \times 10^{-15} \text{ cm}^{2\text{f,b}}$ $\tau_{\text{d,NO}_2}=18 \text{ s}^{\text{f,b}}$
C	O ₃ , NO ₂ , H ₂ O	(R1) to (R5)		$\alpha_{\text{s,0,H}_2\text{O}}=0.4 \times 10^{-3\text{h,a}}$ $\sigma_{\text{H}_2\text{O}}=1.08 \times 10^{-15} \text{ cm}^{2\text{g}}$ $\tau_{\text{d,H}_2\text{O}}=3 \times 10^{-3} \text{ s}^{\text{a}}$

^a Pöschl et al. (2001); ^b Ammann and Pöschl (2007); ^c Stephens et al. (1986); ^d Ammann et al. (1998); ^e Gerecke et al. (1998); ^f Ammann et al. (1997); ^g Nishino (2001); ^h Rogaski et al. (1997)

**Fig. 2.** The temporal evolution of gas-phase component concentrations (**G**), surface component concentrations, and uptake coefficients for the adsorption and surface reaction of O₃ (**A**), the co-adsorption of O₃ and NO₂ (**B**), and the co-adsorption of O₃, NO₂, and H₂O (**C**) following the surface reactions defined in Table 1 is plotted on a logarithmic timescale for day one (left panels) and on a linear timescale for the four following days (right panels).

various places in this paper. We briefly discuss these scenarios when defined, since they involve only minor changes of the scenarios described above.

4 Results and discussion

In this section, we present and discuss the results of the different model scenarios. Section 4.1 focuses on the soot surface chemistry and composition, followed by an account on the characteristic lifetime of the coating substance BaP in Sect. 4.2. In Sect. 4.3, we assess the influence of heterogeneous reactions on the gas-phase O₃ concentration for emission and non-emission scenarios. These results are then compared with the gas-phase O₃ feedback obtained by applying constant uptake coefficients in Sect. 4.4.

4.1 Surface composition

The surface chemistry of scenario A is shown in Fig. 2, panel A. During the first 0.1 min, O₃ adsorbs onto an essentially adsorbate free surface with $\theta_s \approx 0$. This causes the initial plateau of the O₃ uptake coefficient γ_{O_3} where its value is dominated by the adsorption flux, so that $\gamma_{O_3} \approx 0.001 = \alpha_{s,0,O_3}$. When reaching a O₃ surface concentration of $[O_3]_s \approx 1.5 \times 10^{14} \text{ cm}^{-2}$, the surface becomes saturated leading to the first decrease in γ_{O_3} until around 1 min. The subsequent plateau in γ_{O_3} is due to the chemical reaction of O₃ in the sorption layer with BaP in the quasi-static surface layer. As a result, the BaP surface concentration decreases, the reactions product concentration $[Y2]_{ss}$ increases, and O₃ uptake remains constant to sustain the reaction. Further depletion of BaP causes the second decrease of γ_{O_3} at 10 min, followed again by a plateau due to the reaction of O₃ with Y2 that increases the surface concentration of Y3. The same temporal pattern applies for the production of Y4 from the reaction of O₃ with Y3. After the first day, the gas-phase O₃ concentration increases due to the photochemical production from the reactions of the O₃ precursors NO_x and VOCs. This is shown in Fig. 2, panel G, which presents the gas-phase concentrations and diurnal cycles of O₃, NO₂, NO, and HONO corresponding to scenario A. Since the effect of the surface chemistry on the gas phase is negligible in scenario A, B, and C, the temporal evolution of the gas-phase concentrations in scenarios A, B, and C are identical. An increase in gas-phase O₃ concentration results in a larger O₃ uptake according to Eq. (11). However, with $\gamma_{O_3} < 1 \times 10^{-7}$, its magnitude stays below first-day values due to increased surface saturation and the consumption of reactive primary surface components. Within the first day, BaP is decreased by almost 100%, essentially turning off surface reaction (R1) which subsequently slows down or inhibits reactions (R2) to (R5) due to the decrease of educt production. During nighttime, the O₃ adsorption flux decreases due to O₃-depleting reactions and the absence of gas-phase O₃ sources. On the

other hand, high surface saturation leads to an increase in the desorption flux of surface O₃, so that the desorption flux can temporarily exceed the adsorption flux. This results in negative γ_{O_3} -values which represent the direct response to the diurnal cycle of gas-phase O₃ as depicted in Fig. 2, panel G, and are indicated by the discontinuations along the abscissa in Fig. 2, panel A. The value of γ_{O_3} decreases by more than five orders of magnitude and then becomes negative.

The surface chemistry of scenario B is shown in Fig. 2, panel B. In this scenario, two gas-phase species, O₃ and NO₂, adsorb onto the soot surface. Initial adsorption of gas-phase species, chemical consumption of BaP and surface components, and chemical production of surface components proceed similar to scenario A. Although NO₂ gas-phase concentrations are lower, the initial NO₂ uptake exceeds that of O₃ due to a larger accommodation coefficient for NO₂ of $\alpha_{s,0,NO_2} = 0.14$ compared to $\alpha_{s,0,O_3} = 0.001$ for O₃. In comparison to scenario A, the O₃ surface concentration is reduced in scenario B due to the co-adsorption of NO₂. Also concentrations of the other surface components are different compared to the ones in scenario A. The lifetime of Y2 decreases by almost two days due to the added Y5-producing reaction with NO₂. The Y3 concentration is reduced by almost half in comparison to scenario A, since not all Y2 are converted into Y3 anymore. As given in Table 1, the reaction rates for the reactions of NO₂ with Y2 and Y3 are faster than the reaction rates for the reactions of O₃ with Y2 and Y3. Therefore, NO₂ converts Y2 into Y5 and Y3 into HONO faster than O₃ converts Y2 to Y3 and further to Y4. This delays Y4 production by over two days. The proportionality between adsorption flux and gas-phase concentration in Eq. (7) relates the adsorbents' uptake coefficients and surface concentrations to their gas-phase concentrations. This becomes evident after the initial surface saturation at around one minute of simulation time and, more pronounced, after six hours. Since the NO₂ adsorption flux initially exceeds that of O₃, more NO₂ molecules than O₃ molecules are occupying surface sites. Therefore the NO₂ surface concentration exhibits the same temporal evolution as the NO₂ gas-phase concentration, which can be seen by comparing panels B and G in Fig. 2. The O₃ surface concentration increases when surface sites become available from a decrease in the NO₂ surface concentration due to a decrease in the NO₂ gas-phase concentration. The resulting alternating evolution of O₃ and NO₂ surface concentrations also induces an alternating evolution of O₃ and NO₂ uptake coefficients, with maxima ranging from 1×10^{-5} to 1×10^{-4} for γ_{NO_2} , and from 5×10^{-8} to 3×10^{-7} for γ_{O_3} on days two to five. However, these values are three orders of magnitude smaller than the initial uptake coefficients. This indicates that 99.9% of the uptake occurs within the first six hours.

The surface chemistry of scenario C is shown in Fig. 2, panel C. In this scenario, also water vapor, in addition to NO₂ and O₃, co-adsorbs onto the soot surface, but it does not take part in chemical surface reactions. H₂O has a gas-phase

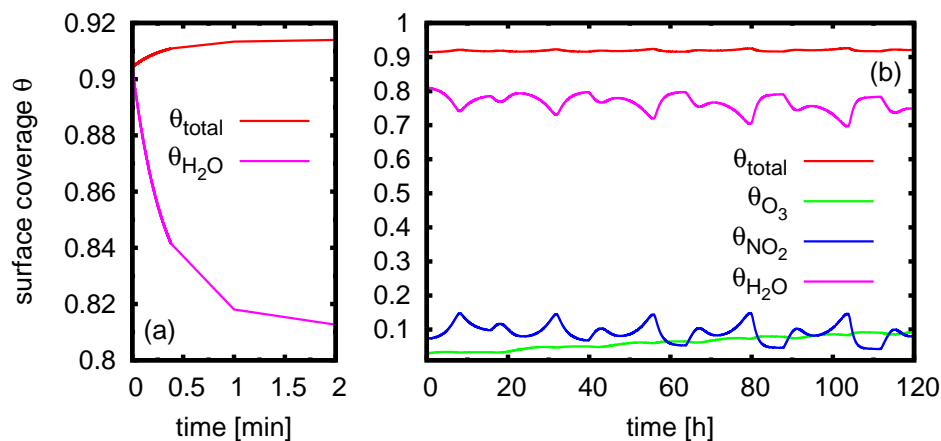


Fig. 3. The temporal evolution of the soot surface coverage θ in scenario C is shown for the first 2 min (a), and for the entire simulation period of five days (b). The total surface coverage is indicated by θ_{total} , and the fractional surface coverages of O₃, NO₂, and H₂O by θ_{O_3} , θ_{NO_2} , and $\theta_{\text{H}_2\text{O}}$, respectively. Input parameters and surface reactions for scenario C are given in Table 1.

concentration of about 20 000 ppmv. This corresponds to 64% RH and is six and eight orders of magnitude larger than the gas-phase concentrations of O₃ and NO₂, respectively. Due to its high partial pressure, H₂O adsorbs rapidly onto the soot surface. Figure 3a shows that the H₂O surface coverage is initially over 90%, but decreases to below 82% within the first 2 min of simulation time. Figure 3b indicates that H₂O constantly occupies about 75% of the total surface for the course of the simulation. This reduces the adsorption fluxes of O₃ and NO₂ and results in a decrease in the surface concentrations and uptake coefficients of O₃ and NO₂ by almost one order of magnitude and half an order of magnitude, respectively, as can be seen by comparison with Fig. 2, panel B. Since O₃ and NO₂ adsorption have little influence on the total surface coverage, their gas-phase uptakes and surface concentrations are not as interdependent as in scenario B. Consequently, both the O₃ and the NO₂ surface concentrations mimic closely their respective gas-phase concentrations, which are depicted in Fig. 2, panel G. Lower surface concentrations of O₃ and NO₂ also result in slower surface reactions, thereby delaying the production of higher order surface components by over half an order of magnitude. For this reason, the uptake coefficients exhibit only two plateaus on the first day, one due to the initial uptake and one governed by the reactions of O₃ with BaP and NO₂ with Y2. On days two to five, the evolution of O₃ and NO₂ uptake coefficients is similar to the one in scenario B, but in comparison to scenario B, maximum γ -values are reduced by up to one order of magnitude.

We investigated the effect of high NO-emissions on the gas phase and particle surface composition of scenario B by increasing the NO emission 10-fold, from 2.68 pptv min⁻¹ to 26.8 pptv min⁻¹. The simulation results are shown in Fig. 4. Figure 4, panel G, shows the temporal evolution of the gas-phase concentrations of O₃, NO₂, NO, and HONO for

this model scenario. While the NO gas-phase concentration increases from 0.2 ppbv to 97 ppbv during the five days simulation period, more NO can react with O₃ to produce NO₂ and O leading to a strong nighttime titration of O₃ from the second to the fifth day. Figure 4, panel B*, presents the soot particle's surface concentrations. As can be seen in Fig. 4, panel B*, the O₃ gas-phase depletion is accompanied by a decrease in the O₃ surface concentration. During periods of O₃ depletion, γ_{O_3} becomes negative, since surface desorption exceeds the reduced adsorption from the gas phase. The overall decrease in the O₃ surface concentration delays the production of the surface component Y4 until the fifth day of the simulation period. The decrease in the O₃ surface coverage yields increases in the NO₂ surface concentration resulting in NO₂ saturation with a maximum surface concentration of $1/\sigma_{\text{NO}_2} = 3 \times 10^{14} \text{ cm}^{-2}$. Although only the NO emission rate was changed compared to scenario B, the particle surface compositions of this scenario and of scenario B are significantly different. While in scenario B (see Fig. 2, panel B) the O₃ surface concentration is almost double the amount of the NO₂ surface concentration at the end of the five day simulation period, the sorption layer surface in the high NO emission scenario is almost entirely filled with NO₂ molecules (see Fig. 4, panel B*). This clearly demonstrates that temporal changes in the gas-phase composition can lead to large differences in the particle surface composition.

The variations in the adsorbents' surface concentrations and uptake coefficients after the first day of the simulation period exemplify the differences to uptake scenarios that do not account for a dynamic gas-phase chemistry, such as the Models Systems Solid 1 and 2 discussed in Ammann and Pöschl (2007). However, as shown in Fig. 2, variations in the adsorbents' gas-phase concentrations have a direct effect on the adsorbents' surface concentrations and, consequently, on their uptake coefficients. By accounting for

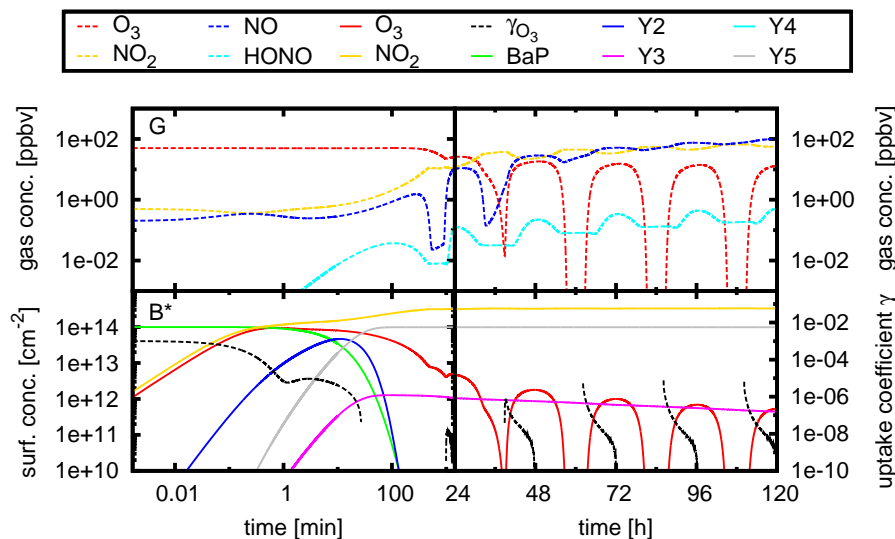


Fig. 4. The temporal evolution of gas-phase component concentrations (G), surface component concentrations, and uptake coefficients for scenario B* are shown and plotted on a logarithmic timescale for day one (left panels) and on a linear timescale for the four following days (right panels). Scenario B* corresponds to scenario B with a 10-fold increase of the NO emission rates.

variable gas-phase concentrations in our coupled PRA framework, we can resolve variations in the uptake coefficient over atmospherically relevant time scales and study the effect of different gas-phase scenarios on the particle surface chemistry.

4.2 BaP lifetime

The consumption of the soot's BaP coating can be regarded as an initial surface oxidation process due to the reaction with O₃ and NO₂. The efficiency of the heterogeneous kinetics of this oxidation processes can be quantified by the BaP half-life. Figure 5 shows the temporal evolution of the BaP concentration for scenarios A, B, C, and scenario C* with the BaP half-lives highlighted by the intersection with the horizontal dotted black line. Scenario C* represents the co-adsorption of O₃ and H₂O following the surface reactions (R1) to (R3) as given in Table 1. It is meant to serve as an additional comparison to scenario A to identify the influence of the co-adsorption of H₂O. Figure 5 indicates that the half-life of BaP surface molecules in scenario A is about 4 min. The addition of the co-adsorbing species NO₂ in scenario B extends the half-life by 54% to 6.2 min. Taking into account H₂O physisorption and atmospheric relative humidity of 64% in scenario C increases the half-life of BaP to 32.5 min as indicated in Fig. 5. Without the NO₂ co-adsorption in scenario C*, the BaP half-life is 30 min, 10% less than in scenario C. This indicates that the H₂O co-adsorption is responsible for over 90% of the increase in BaP half-life between scenarios A and C. The reason for this is the rapid adsorption of H₂O on the surface where it occupies a

large portion of the available surface sites resulting in a high fractional surface coverage of H₂O, as illustrated in Fig. 3. The reactive surface sites occupied by H₂O are not available anymore for the adsorption of O₃ and subsequent BaP consumption via surface reaction (R1). Compared to scenarios A and B, the co-adsorption of water vapor leads to a more than five-fold increase in BaP half-life between scenarios C and B, and more than a seven-fold increase between scenarios C* and A.

The sensitivity of the BaP half-life on the adsorption of H₂O is influenced by the H₂O concentration and therefore by RH. Figure 6 shows that the BaP half-life increases linearly with RH. An increase from 0% RH to 25% RH results in an almost threefold increase in the BaP half-life from 6 min to 17 min for scenario C. Also shown in Fig. 6 are the half-lives of scenarios P and P*. Scenario P* represents BaP half-lives as a function of RH derived from experimental data from the ozonolysis of soot coated with BaP (Pöschl et al., 2001). Scenario P represents our modeling results using the experimental conditions of Pöschl et al. (2001) as input parameters. These are a 30 ppbv constant gas-phase O₃ concentration, an initial BaP surface concentration of $1.8 \times 10^{13} \text{ cm}^{-2}$, a temperature of 296 K, and O₃ and H₂O as adsorbing species. Other input parameters are identical to the ones listed in Table 1. Figure 6 shows that the simulated BaP half-lives in scenario P are slightly longer than the ones inferred from laboratory measurements (Pöschl et al., 2001) given by scenario P*. The simulated BaP half-lives in scenario P are 5.8 min for 0% RH, 22.5 min for 25% RH, and 56 min for 75% RH. The BaP half-lives in scenario P* as derived by Pöschl et al. (2001) are 5 min for 0% RH, 18 min for 25%, and 45 min for 75%

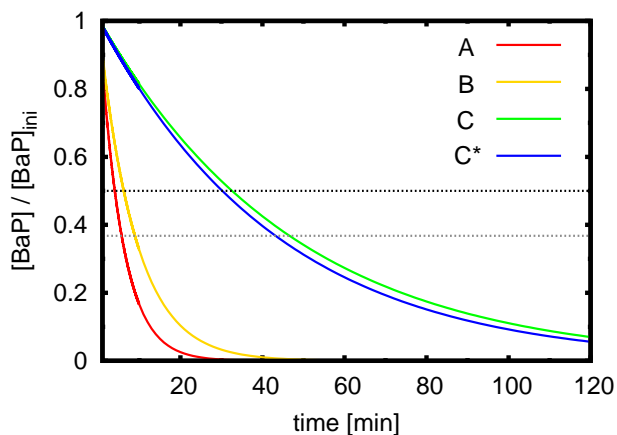


Fig. 5. The temporal evolution of the ratio of actual BaP surface concentration to initial BaP concentration is shown for scenarios A, B, C, and C*. Scenario A represents the adsorption of O₃, scenario B the co-adsorption of O₃ and NO₂, scenario C the co-adsorption of O₃, NO₂, and H₂O, and scenario C* the co-adsorption of O₃ and H₂O. Scenarios A, B, and C follow the surface reactions given in Table 1; scenario C* follows the surface reactions (R1) to (R3) given in Table 1. The intersection with the horizontal dotted lines indicate BaP half-life (dotted black line) and BaP lifetime (dotted grey line).

RH. Reasons for the longer simulated lifetimes in scenario P could be parameter sensitivity or physio-chemical processes that were not accounted for in our model approach. Regarding the former, a 20% reduction in the value for the effective molecular cross section of H₂O would result in half-lives in agreement with the measurements of Pöschl et al. (2001). Regarding the latter, physiochemical processes that are not captured in our model framework are, e.g. the diffusion of adsorbents through surface H₂O which could lead to surface oxidation and a reduction in the BaP half-life even though most reactive sites are occupied by H₂O. Also, changes in the soot particle's hydrophilicity could result in changes of the residence time of surface H₂O, subsequently affecting particle oxidation. A variation of the H₂O desorption time, $\tau_{\text{H}_2\text{O}}$, of about $\pm 10\%$ due to possible changes in particle hydrophilicity changes the BaP lifetime by about ± 5 min.

4.3 Feedback on the gas-phase O₃ concentration with differing uptake and emission scenarios

In this section, we assess the gas-phase O₃ feedback from scenarios A, B, C, and from the emission scenarios A_{4x}, B_{4x}, C_{4x}, and A_{24x}, B_{24x}, C_{24x}. Figure 7 shows the temporal evolution of the gas-phase O₃ concentrations in these scenarios and a base scenario which does not include any heterogeneous reactions on soot. The diurnal cycle of gas-phase O₃ and the potential decreases in the gas-phase O₃ concentration due to the heterogeneous reactions implemented in our model scenarios can be clearly identified.

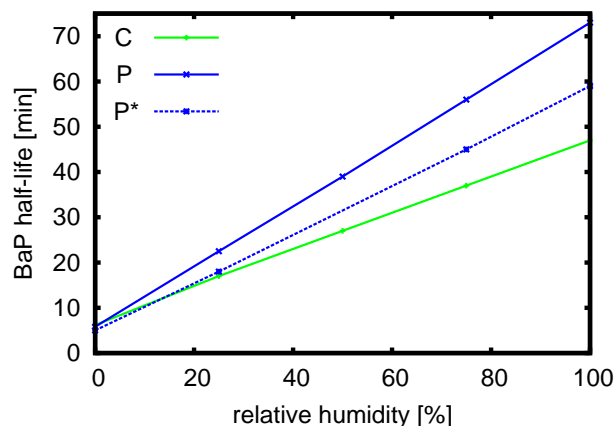


Fig. 6. The BaP half-life is plotted as a function of relative humidity for scenarios C, P, and P*. Scenario C represents the co-adsorption of O₃, NO₂, and H₂O following the surface reactions given in Table 1 with an initial gas-phase O₃ concentration of 50 ppbv, an initial BaP surface concentration of $1 \times 10^{14} \text{ cm}^{-2}$, and a temperature of 298.15 K. Scenario P represents the co-adsorption of O₃ and H₂O following surface Reactions (R1) to (R3) from Table 1 with a constant gas-phase O₃ concentration of 30 ppbv, an initial BaP surface concentration of $1.8 \times 10^{13} \text{ cm}^{-2}$, and a temperature of 296 K corresponding to the boundary conditions of an aerosol flow tube experiment conducted by Pöschl et al. (2001). Scenario P* represents the experimentally derived BaP half-lives from the aerosol flow tube experiment (Pöschl et al., 2001) with the same boundary conditions as used in scenario P.

The gas-phase uptake in scenarios A, B, and C cause no significant decrease in the gas-phase O₃ concentration with respect to the base scenario. Detail 1 in Fig. 7 resolves the differences among scenarios A, B, C. The strongest O₃ depletion among these scenarios is 0.33 ppbv in scenario B which is less than 2% in comparison to the base scenario after the five days modeling period. The difference to the weakest O₃ depleting scenario C is less than 1%. This insignificance of the gas-phase O₃ feedback from the non-emission scenarios is in agreement with previous studies (Kamm et al., 1999; Disselkamp et al., 2000; Nienow and Roberts, 2006) which considered O₃ depletion on soot surfaces as probably negligible under conditions relevant to the upper troposphere and lower stratosphere.

Figure 7 shows a larger gas-phase O₃ reduction for the low emission scenarios A_{4x}, B_{4x}, and C_{4x} in comparison to the non-emission scenarios A, B, C and the base scenario. Detail 2 in Fig. 7 indicates the strongest O₃ reduction for scenario B_{4x}, in which the O₃ concentration is 7.88 ppbv or 4.8% less than in the base scenario after the five days modeling period. The difference in O₃ concentration between scenarios B_{4x} and A_{4x} is less than 1%. In scenario C_{4x}, the O₃ concentration is decreased by 2.6% with respect to the base scenario, which is almost half the decrease of scenario B_{4x}.

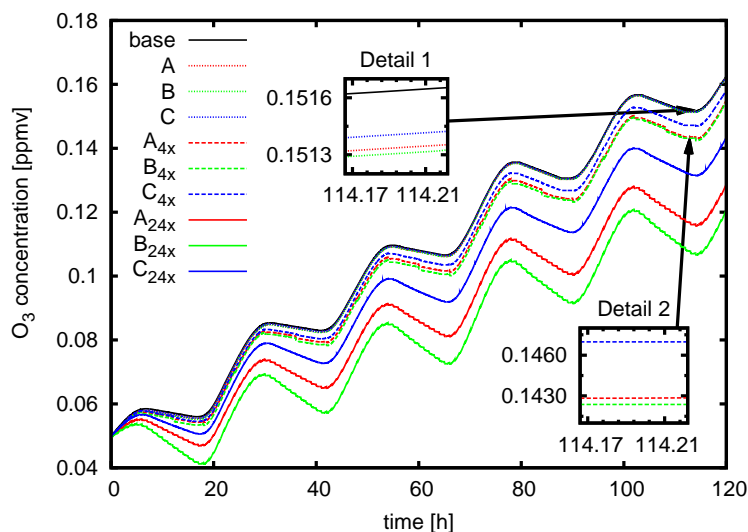


Fig. 7. The temporal evolution of the gas-phase O₃ concentration is shown for a base scenario with no heterogeneous chemistry, for the model scenarios A, B, C, and the corresponding low and high emission scenarios A_{4x}, B_{4x}, C_{4x} and A_{24x}, B_{24x}, C_{24x}, respectively. Detail 1 shows an enlarged view of the results of the base scenario and model scenarios A, B, and C. Detail 2 shows an enlarged view of the results for the low emissions scenarios A_{4x}, B_{4x}, C_{4x}. Input parameters for the A, B, and C-scenarios are given in Table 1.

The high emission scenarios A_{24x}, B_{24x}, and C_{24x} exhibit the largest O₃ reductions. Figure 7 shows the lowest O₃ concentration for scenario B_{24x}, which is 41.6 ppbv or 25.6% less than the O₃ concentration for the base scenario after the five days modeling period. The scenarios A_{24x} and C_{24x} exhibit a decrease in O₃ concentration with respect to the base scenario of 33.8 ppbv and 19.2 ppbv, respectively. These reductions in the tropospheric O₃ concentration indicate that these heterogeneous reactions may have an impact on urban O₃ concentrations.

Figure 7 also shows clear differences in O₃ concentrations between the specific co-adsorption scenarios. The scenarios C, C_{4x}, and C_{24x} are associated with the least O₃ depletion in comparison to the A and B-scenarios. This is due to the co-adsorption of water vapor which hinders direct O₃ uptake by constantly occupying over 75% of the total reactive surface as discussed in Sect. 4.1. In terms of gas-phase O₃ reduction, the A-scenarios, in which only O₃ is taken up, do not deplete gas-phase O₃ concentrations as much as the B-scenarios, in which less O₃ is taken up by the soot surface directly. However, the additional NO₂ uptake in the B-scenarios affects the gas-phase NO_x-O₃ production cycle leading to a lower O₃ concentration than in cases with no NO₂ uptake. Consequently, no clear relationship between the number of adsorbing species and the resulting O₃ depletion can be established. As can also be seen from Fig. 7, the relative difference in gas-phase O₃ concentrations between the A, B, and C-scenarios increases disproportionately from the non-emission and low emission scenarios to the high emission scenarios. This highlights the non-linear behavior of the gas-phase O₃ depletion due to the co-adsorption

of the interdependent species O₃ and NO₂, and the rapid co-adsorption of H₂O.

Since there is a wide range of measured uptake coefficients for NO₂ on soot, ranging from smaller than 4×10^{-8} to 0.12 (Aubin and Abbatt, 2007), we simulated the B-scenarios with accommodation coefficients of $\alpha_{\text{NO}_2} = 10^{-6}$ (Kleffmann et al., 1999) and $\alpha_{\text{NO}_2} = 10^{-3}$ (Kirchner et al., 2000). These lower initial uptake coefficients yield, within 1 ppbv, the same gas-phase feedback as the A-scenarios, which have no NO₂ co-adsorption implemented. Thus, the gas-phase feedback from the co-adsorption of NO₂ obeying an accommodation coefficient smaller than 10^{-3} is negligible.

It should be noted that the feedback on the gas-phase O₃ concentration from the desorption of HONO in surface reaction (R5) given in Table 1 was found to be negligible for all model scenarios due to the small production rate in relation to gas-phase production. The HONO production rate from desorption is $0.22 \text{ ppmv}^{-1} \text{ min}^{-1}$ which is five orders of magnitude smaller than the gas-phase production rate of NO with OH. In the mornings, the gas-phase HONO production temporarily decreases due to low OH concentrations, but surface desorption is still one order of magnitude smaller than the gas-phase production and thus does not exert a significant influence.

The error in both emission scenarios from neglecting gas-phase uptake on disregarded surface sites can be estimated with reference to Sect. 4.1 and Fig. 2. Figure 2 shows that, for each adsorption scenario, the uptake coefficients decrease by more than three orders of magnitude or 99.9% within the first six hours of simulation time. Therefore, the error in the low emission scenarios from neglecting gas-phase uptake on soot

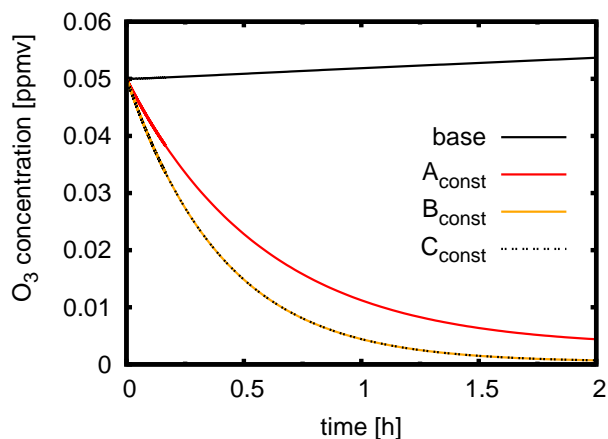


Fig. 8. The temporal evolution of the gas-phase O₃ concentration is shown for a base scenario with no heterogeneous chemistry and for the constant uptake scenarios A_{const}, B_{const}, C_{const}. Scenarios A_{const}, B_{const}, C_{const} use constant uptake coefficients of $\gamma_{\text{O}_3}=1\times 10^{-3}$ (Stephens et al., 1986; Pöschl et al., 2001), $\gamma_{\text{NO}_2}=0.14$ (Gerecke et al., 1998; Ammann and Pöschl, 2007), and $\gamma_{\text{H}_2\text{O}}=0.4\times 10^{-3}$ (Rogaski et al., 1997; Pöschl et al., 2001) but are otherwise equivalent to scenarios A, B, and C as defined in Table 1.

surfaces that are older than six hours is not significant. After one hour of simulation time, the uptake coefficients fall by one to two orders of magnitude, depending on the scenario. Thus, up to 10% of gas-phase uptake is neglected in the high emission scenarios due to an hourly replenishing time, which results in a small underestimate of the total gas-phase uptake.

In the next section, we compare the gas-phase feedback from heterogeneous chemistry obtained in this section for the dynamic uptake coefficient approach with the gas-phase feedback obtained from the use of constant uptake coefficients.

4.4 Gas-phase O₃ feedback for constant uptake parameterizations

To study the gas-phase feedback from a heterogeneous modeling approach employing constant uptake coefficients, we implement the experimentally determined constant uptake coefficients of $\gamma_{\text{O}_3}=1\times 10^{-3}$ for O₃ uptake (Pöschl et al., 2001), $\gamma_{\text{NO}_2}=0.14$ for NO₂ uptake (Gerecke et al., 1998), and $\gamma_{\text{H}_2\text{O}}=0.4\times 10^{-3}$ for the uptake of water vapor (Rogaski et al., 1997) into the non-emission scenarios A, B, and C. These γ_{X_i} -values represent initial uptake coefficients that were previously implemented in our model as accommodation coefficients. The gas-phase loss is computed according to Eq. (12) with the same input parameters, particle surface concentration and gas-phase concentrations that were previously used in scenarios A, B, and C. We denote these constant uptake coefficient scenarios by A_{const}, B_{const}, C_{const}.

The application of constant uptake coefficients reduced the computation time by a factor of about 18 compared to a dynamic uptake approach and needed roughly the same time as a simulation without any heterogeneous reactions implemented.

Figure 8 shows the temporal evolution of the gas-phase O₃ concentration for scenarios A_{const}, B_{const}, C_{const} and for a base scenario without heterogeneous chemistry. After two hours of modeling time, the gas-phase O₃ concentration in the constant uptake coefficient scenarios A_{const}, B_{const}, and C_{const} falls by more than one order of magnitude and is approaching zero. This fast depletion of O₃ is due to the fact that the gas-phase uptake is not limited by surface saturation, which otherwise would reduce the uptake coefficients. The uptake is now solely determined by the adsorbents' constant uptake coefficients, their molecular velocities, and their gas-phase concentrations via Eq. (12). This results also in a different ordering of scenarios in terms of their O₃ depletion efficiency when compared to the dynamic uptake scenarios. Scenario A_{const} shows the least gas-phase O₃ depletion, since it employs the lowest uptake coefficient. Scenarios B_{const} and C_{const} show the same O₃ depletion, since in this constant uptake coefficient approach, the co-adsorption of water vapor in scenario C_{const} does not reduce the gas-phase uptake of O₃ and NO₂ which therefore is the same as in scenario B_{const}.

Clearly, these constant uptake coefficient scenarios do not represent the underlying physical and chemical processes and result in an unrealistically high gas-phase O₃ depletion which may not describe typical urban plume conditions.

In addition to using the initial uptake coefficients as constant uptake values, we also attempted to parameterize the uptake process by several time-specific uptake values modeled after the temporal evolution of the uptake coefficients as shown in Fig. 2. Neither a 3-step uptake parametrization, nor a 2-step one using an initial uptake value from laboratory measurements and subsequent values from our model was successful in capturing the O₃ depleting effect. Application of a single constant uptake value for each adsorbent yielded acceptable agreement with the gas-phase O₃ concentration of the respective model scenarios if an uptake value was chosen significantly different from the laboratory measurements and model results. However, this approach is only successful for a certain time frame and certain boundary conditions, such as initial gas-phase concentrations. Furthermore, the adsorbent-specific uptake values determined in such a way, could not be used to capture the combined effect on the O₃ concentration of two or more adsorbents. Thus, the uptake values obtained in this manner are heavily scenario dependent and therefore of little use in general atmospheric models. These difficulties in obtaining a simplified and thus computationally more efficient description of the uptake process clearly indicate the underlying complexity of the involved physical-chemical mechanisms, emphasizing the need for a detailed modeling framework to accurately resolve the uptake process.

5 Conclusions

The PRA framework (Pöschl et al., 2007), which allows a dynamic uptake coefficient treatment, was coupled to a box model version of the gas-phase solver RADM2 (Stockwell et al., 1990) to model heterogeneous reactions of O₃, NO₂, and water vapor on soot coated with benzo[a]pyrene for a period of five days. Gas-phase reactions and emissions were based on an urban plume scenario (Kuhn et al., 1998). This allowed us to study, in detail, the heterogeneous kinetics and its dependency on diurnal changes in gas-phase composition due to photochemical processes.

A detailed analysis of surface chemistry showed that the O₃ and NO₂ uptake coefficients vary by more than five orders of magnitude due to competition for reactive surface sites and changes in gas-phase composition. Within the first six hours of simulation time, the uptake coefficients decrease by more than three orders of magnitude or 99.9%. From day two to five, periodic peaks of the uptake coefficient follow the diurnal cycle of the adsorbents' gas-phase concentrations.

The half-life of BaP was found to increase with the number of co-adsorbing species. Physisorption of water vapor increased the BaP half-life by a factor of five to seven by permanently occupying about 75% of the surface and thereby delaying the surface reactions of O₃ and NO₂. The BaP half-life increases linearly with RH and the linearity is preserved under changes in O₃ and BaP concentrations, temperature, and number of adsorbing species. Our results show that even at low RH, the adsorption of water vapor can play a major role in the soot surface chemistry. An increase from 0% RH to 25% RH increases the BaP half-life by a factor of three.

This study indicates the importance of the co-adsorption of water vapor for heterogeneous chemistry also for aerosol particles other than soot coated with BaP. Since BaP belongs to the group of polycyclic aromatic hydrocarbons which are known to be hydrophobic (Rogge et al., 1993), an even greater impact of water vapor co-adsorption on surface chemistry can be expected for more hydrophilic surfaces. While our model does not capture changes in hydrophilicity, it assesses surface oxidation which is thought to influence the activation of tropospheric aerosols as cloud condensation nuclei (CCN) (Rudich, 2003; Rudich et al., 2007; Kanakidou et al., 2005; Petters et al., 2006; Shilling et al., 2007). Our modeling approach is able to estimate surface oxidation times, such as the BaP half-life, in an atmospheric context and may therefore be used in part to derive CCN activation times.

We also assessed the feedback of heterogeneous uptake on the gas-phase O₃ concentration. The different co-adsorption scenarios with no soot emissions implemented showed no significant feedback on the gas-phase composition. However, two emission scenarios in which reactive surface sites are replenished every six hours and every hour induced significant changes in the gas-phase O₃ concentration. The largest O₃ depletions were observed for the hourly high

emission scenario with a reduction in O₃ concentration of up to 41.6 ppbv or 25% for the co-adsorption of O₃ and NO₂. It also resulted in a reduction of 33.8 ppbv or 21% for the scenario with the adsorption of O₃, and of 19.2 ppbv or 11.8% for the scenario with the co-adsorption of O₃, NO₂, and water vapor. In comparison, the low emission scenarios replenishing reactive sites every six hours showed a decrease in gas-phase O₃ concentration of maximum 7.8 ppbv or 5%. Hence, our conceptual study employing soot particles in an urban environment indicates that heterogeneous chemistry has the potential to significantly alter the gas-phase composition.

Our model results indicated that the uptake is sensitive to the co-adsorbing species and their interactions with each other. The scenario with the most O₃ uptake from the exclusive adsorption of O₃ is surpassed in overall gas-phase O₃ reduction by the scenario in which O₃ and NO₂ co-adsorb. This is due to the additional O₃ reduction induced by the gas-phase reactions between O₃ and NO₂. This exemplifies the non-linear feedbacks obtained from a co-adsorption scheme.

Although heterogeneous reactions can be an important source for nitrous acid (HONO) (Stemmler et al., 2006), the desorption of HONO from surface reactions of NO₂ on soot particles was found to be negligible for the gas-phase O₃ concentration.

We compared the dynamic uptake coefficient approach with a constant uptake coefficients approach. The use of experimentally determined reactive uptake coefficients which were kept constant in these model scenarios led to an almost complete gas-phase O₃ depletion after two hours of modeling time which is highly unrealistic for an urban plume scenario. Since surface conditions and reactions were not related to the uptake dynamics in these constant uptake coefficient scenarios, the co-adsorption of water vapor had no impact on the efficiency of gas-phase O₃ depletion which ignores the underlying physical and chemical picture and is in contrast to the results from the dynamic uptake coefficient approach.

It should be noted that modeling studies used constant uptake coefficients, but employed consumable reactive sites on the soot surface to account for surface passivation (Aklilu and Michelangeli, 2004). This approach yields a more physical picture of the gas-phase uptake, but it still lacks the accurate description of the heterogeneous kinetics involving the interdependence of gas-phase and adsorbed surface species. Our study showed that the superposition of fixed reactive uptake coefficients, despite being experimentally determined, can result in erroneous results for the overall uptake efficiency and thus gas-phase composition.

Other modeling studies used empirical parameterizations of the uptake coefficient as a function of relative humidity, temperature, and aerosol type (Evans and Jacob, 2005; Davis et al., 2008). As such, the parametrization of N₂O₅ hydrolysis yields gas-phase concentrations in good agreement with climatological observations (Evans and Jacob, 2005). This may be due to the fact that the N₂O₅ hydrolysis in aqueous aerosol particles follows an absorption type reaction

mechanism (Hanson and Ravishankara, 1991; Knopf et al., 2007; Cosman et al., 2008), i.e. the uptake can be dominated by dissolution of the gas-phase species into the particle governed by Henry's law constant and by subsequent reaction in the bulk (Finlayson-Pitts and Pitts, 2000). In such heterogeneous processes, gas-phase species do not compete for reactive surface sites, which therefore have no effect on the subsequent uptake. In contrast, heterogeneous reactions following adsorption kinetics may predominantly occur at the surface of solid or crystalline particles (Rudich, 2003) and aqueous surfaces coated by an organic surfactant (Donaldson and Vaida, 2006). This limits the available number of reactive surface sites in comparison to the bulk liquid. Therefore, higher order reactive uptake processes such as Langmuir-Hinshelwood surface reactions will not be correctly represented by the application of constant reactive uptake coefficients.

This study clearly emphasizes the need for laboratory data of physical and chemical parameters for atmospherically relevant adsorbents and aerosols to predict, in detail, the effects of heterogeneous chemistry on the gas-phase and aerosol composition.

Acknowledgements. The authors are grateful for helpful discussions with M. Ammann.

Edited by: V. F. McNeill

References

- Aklilu, Y. A. and Michelangeli, D. V.: Box model investigation of the effect of soot particles on ozone downwind from an urban area through heterogeneous reactions, *Environ. Sci. Technol.*, 38, 5540–5547, doi:10.1021/es035079x, 2004.
- Ammann, M. and Pöschl, U.: Kinetic model framework for aerosol and cloud surface chemistry and gas-particle interactions - Part 2: Exemplary practical applications and numerical simulations, *Atmos. Chem. Phys.*, 7, 6025–6045, 2007, <http://www.atmos-chem-phys.net/7/6025/2007/>.
- Ammann, M., Rössler, E., Baltensperger, U., and Kalberer, M.: Heterogeneous reaction of NO₂ on bulk soot samples, *Laboratory of Radio- and Environmental Chemistry Annual Report 1997*, Paul Scherrer Institute, Switzerland, 24, 1997.
- Ammann, M., Kalberer, M., Jost, D., Tobler, L., Rössler, E., Piguet, D., Gaggeler, H., and Baltensperger, U.: Heterogeneous production of nitrous acid on soot in polluted air masses, *Nature*, 395, 157–160, 1998.
- Arens, F., Gutzwiller, L., Baltensperger, U., Gaggeler, H., and Ammann, M.: Heterogeneous reaction of NO₂ on diesel soot particles, *Environ. Sci. Technol.*, 35, 2191–2199, 2001.
- Arens, F., Gutzwiller, L., Gaggeler, H. W., and Ammann, M.: The reaction of NO₂ with solid anthracene (1,2,10-trihydroxy-anthracene), *Phys. Chem. Chem. Phys.*, 4, 3684–3690, doi:10.1039/b201713j, 2002.
- Atkinson, R., Baulch, D. L., Cox, R. A., Crowley, J. N., Hampson Jr., R. F., Kerr, J. A., Rossi, M. J., and Troe, J.: Summary of Evaluated Kinetic and Photochemical Data for Atmospheric Chemistry, Web Version, www.iupac-kinetic.ch.cam.ac.uk, last access: 27 March 2009, University of Cambridge, UK, 2001.
- Aubin, D. G. and Abbatt, J. P. D.: Interaction of NO₂ with hydrocarbon soot: Focus on HONO yield, surface modification, and mechanism, *J. Phys. Chem. A*, 111, 6263–6273, doi:10.1021/jp068884h, 2007.
- Bernstein, J. A., Alexis, N., Barnes, C., Bernstein, I. L., Bernstein, J. A., Nel, A., Peden, D., Diaz-Sanchez, D., Tarlo, S. M., and Williams, P. B.: Health effects of air pollution, *J. Allergy Clin. Immunol.*, 114, 1116–1123, doi:10.1016/j.jaci.2004.08.030, 2004.
- Bertram, A. K., Ivanov, A. V., Hunter, M., Molina, L. T., and Molina, M. J.: The reaction probability of OH on organic surfaces of tropospheric interest, *J. Phys. Chem. A*, 105, 9415–9421, 2001.
- Bey, I., Jacob, D. J., Yantosca, R. M., Logan, J. A., Field, B. D., Fiore, A. M., Li, Q. B., Liu, H. G. Y., Mickley, L. J., and Schultz, M. G.: Global modeling of tropospheric chemistry with assimilated meteorology: Model description and evaluation, *J. Geophys. Res.-Atmos.*, 106, 23073–23095, 2001.
- Bond, T. C., Streets, D. G., Yarber, K. F., Nelson, S. M., Woo, J. H., and Klimont, Z.: A technology-based global inventory of black and organic carbon emissions from combustion, *J. Geophys. Res.-Atmos.*, 109, D14203, doi:10.1029/2003JD003697, 2004.
- Brown, S. S., Ryerson, T. B., Wollny, A. G., Brock, C. A., Peltier, R., Sullivan, A. P., Weber, R. J., Dube, W. P., Trainer, M., Meagher, J. F., Fehsenfeld, F. C., and Ravishankara, A. R.: Variability in nocturnal nitrogen oxide processing and its role in regional air quality, *Science*, 311, 67–70, doi:10.1126/science.1120120, 2006.
- Chang, J. S., Brost, R. A., Isaksen, I. S. A., Madronich, S., Middleton, P., Stockwell, W. R., and Walcek, C. J.: A Three-Dimensional Eulerian Acid Deposition Model – Physical Concepts and Formulation, *J. Geophys. Res.-Atmos.*, 92, 14681–14700, 1987.
- Cheung, J. L., Li, Y. Q., Boniface, J., Shi, Q., Davidovits, P., Worsnop, D. R., Jayne, J. T., and Kolb, C. E.: Heterogeneous interactions of NO₂ with aqueous surfaces, *J. Phys. Chem. A*, 104, 2655–2662, 2002.
- Choi, W. and Leu, M. T.: Nitric acid uptake and decomposition on black carbon (soot) surfaces: Its implications for the upper troposphere and lower stratosphere, *J. Phys. Chem. A*, 102, 7618–7630, 1998.
- Cosman, L. M., Knopf, D. A., and Bertram, A. K.: N₂O₅ reactive uptake on aqueous sulfuric acid solutions coated with branched and straight-chain insoluble organic surfactants, *J. Phys. Chem. A*, 112, 2386–2396, 2008.
- Crutzen, P. J. and Arnold, F.: Nitric-acid cloud formation in the cold antarctic stratosphere – a major cause for the springtime ozone hole, *Nature*, 324, 651–655, 1986.
- Danckwerts, P. V.: Absorption by simultaneous diffusion and chemical reaction into particles of various shapes and into falling drops, *T. Faraday Soc.*, 47, 1014–1023, 1951.
- Davis, J. M., Bhave, P. V., and Foley, K. M.: Parameterization of N₂O₅ reaction probabilities on the surface of particles containing ammonium, sulfate, and nitrate, *Atmos. Chem. Phys.*, 8, 5295–5311, 2008, <http://www.atmos-chem-phys.net/8/5295/2008/>.
- Dentener, F. J., Carmichael, G. R., Zhang, Y., Lelieveld, J., and Crutzen, P. J.: Role of mineral aerosol as a reactive surface in

- the global troposphere, *J. Geophys. Res.-Atmos.*, 101, 22869–22889, 1996.
- Derwent, R. G. and Jenkin, M. E.: Hydrocarbons and the Long-range Transport of Ozone and PAN Across Europe, *Atmos. Environ. A-Gen.*, 25, 1661–1678, 1991.
- Disselkamp, R. S., Carpenter, M. A., Cowin, J. P., Berkowitz, C. M., Chapman, E. G., Zaveri, R. A., and Laulainen, N. S.: Ozone loss in soot aerosols, *J. Geophys. Res.-Atmos.*, 105, 9767–9771, 2000.
- Donaldson, D. J. and Vaida, V.: The Influence of Organic Films at the Air-Aqueous Boundary on Atmospheric Processes, *Chem. Rev.*, 106, 1445–1461, doi:10.1021/cr040367c, 2006.
- Dymarska, M., Murray, B. J., Sun, L. M., Eastwood, M. L., Knopf, D. A., and Bertram, A.: Deposition ice nucleation on soot at temperatures relevant for the lower troposphere, *J. Geophys. Res.-Atmos.*, 111, D04204, doi:10.1029/2005JD006627, 2006.
- EPA, U. S.: 2006 Edition of the Drinking Water Standards and Health Advisories, US Environmental Protection Agency, Washington, DC, epa 822-r-06-013 edn., 18 pp., 2006a.
- EPA, U. S.: Air Quality Criteria for Ozone and Related Photochemical Oxidants (Final), US Environmental Protection Agency, Washington, DC, epa/600/r-05/004af-cf edn., 821 pp., 2006b.
- Evans, M. J. and Jacob, D. J.: Impact of new laboratory studies of N₂O₅ hydrolysis on global model budgets of tropospheric nitrogen oxides, ozone, and OH, *Geophys. Res. Lett.*, 32, L09813, doi:10.1029/2005GL022469, 2005.
- Finlayson-Pitts, B. J. and Pitts, J. N.: Tropospheric air pollution: Ozone, airborne toxics, polycyclic aromatic hydrocarbons, and particles, *Science*, 276, 1045–1052, 1997.
- Finlayson-Pitts, B. J. and Pitts, J. N.: Chemistry of the Upper and Lower Atmosphere, Academic Press, San Diego, 969 pp., 2000.
- Franze, T., Weller, M. G., Niessner, R., and Pöschl, U.: Enzyme immunoassays for the investigation of protein nitration by air pollutants, *Analyst*, 128, 824–831, doi:10.1039/b303132b, 2003.
- Franze, T., Weller, M. G., Niessner, R., and Pöschl, U.: Protein nitration by polluted air, *Environ. Sci. Technol.*, 39, 1673–1678, doi:10.1021/es0488737, 2005.
- Fuchs, N. A. and Sutugin, A. G.: High-dispersed aerosols, in: Topics in current aerosol research., edited by: Hidy, G. M. and Brock, J. R., Pergamon, New York, 1971.
- Gerecke, A., Thielmann, A., Gutzwiller, L., and Rossi, M. J.: The chemical kinetics of HONO formation resulting from heterogeneous interaction of NO₂ with flame soot, *Geophys. Res. Lett.*, 25, 2453–2456, 1998.
- Grell, G. A., Peckham, S. E., Schmitz, R., McKeen, S. A., Frost, G., Skamarock, W. C., and Eder, B.: Fully coupled “online” chemistry within the WRF model, *Atmos. Environ.*, 39, 6957–6975, 2005.
- Gross, S. and Bertram, A. K.: Reactive Uptake of NO₃, N₂O₅, NO₂, HNO₃, and O₃ on Three Types of Polycyclic Aromatic Hydrocarbon Surfaces, *J. Phys. Chem. A*, 112, 3104–3113, 2008.
- Gross, S. and Bertram, A. K.: Products and kinetics of the reactions of an alkane monolayer and a terminal alkene monolayer with NO₃ radicals, *J. Geophys. Res.-Atmos.*, 114, D02307, doi:10.1029/2008JD010987, 2009.
- Hanson, D. R. and Ravishankara, A. R.: The reaction probabilities of ClONO₂ and N₂O₅ on 40-percent to 75-percent sulfuric-acid-solutions, *J. Geophys. Res.-Atmos.*, 96, 17307–17314, 1991.
- Hearn, J. D. and Smith G. D.: A mixed-phase relative rates technique for measuring aerosol reaction kinetics, *Geophys. Res. Lett.*, 33, L17805, doi:10.1029/2006GL026963, 2006.
- Homann, K. H.: Fullerenes and soot formation – New pathways to large particles in flames, *Angew. Chem., Int. Ed.*, 37, 2435–2451, 1998.
- Kamm, S., Mohler, O., Naumann, K. H., Saathoff, H., and Schurath, U.: The heterogeneous reaction of ozone with soot aerosol, *Atmos. Environ.*, 33, 4651–4661, 1999.
- Kanakidou, M., Seinfeld, J. H., Pandis, S. N., Barnes, I., Dentener, F. J., Facchini, M. C., Van Dingenen, R., Ervens, B., Nenes, A., Nielsen, C. J., Swietlicki, E., Putaud, J. P., Balkanski, Y., Fuzzi, S., Horth, J., Moortgat, G. K., Winterhalter, R., Myhre, C. E. L., Tsigaridis, K., Vignati, E., Stephanou, E. G., and Wilson, J.: Organic aerosol and global climate modelling: a review, *Atmos. Chem. Phys.*, 5, 1053–1123, 2005, <http://www.atmos-chem-phys.net/5/1053/2005/>.
- Karagulian, F., Santschi, C., and Rossi, M. J.: The heterogeneous chemical kinetics of N₂O₅ on CaCO₃ and other atmospheric mineral dust surrogates, *Atmos. Chem. Phys.*, 6, 1373–1388, 2006, <http://www.atmos-chem-phys.net/6/1373/2006/>.
- Kirchner, U., Scheer, V., and Vogt, R.: FTIR spectroscopic investigation of the mechanism and kinetics of the heterogeneous reactions of NO₂ and HNO₃ with soot, *J. Phys. Chem. A*, 104, 8908–8915, 2000.
- Kleffmann, J., Becker, K. H., Lackhoff, M., and Wiesen, P.: Heterogeneous conversion of NO₂ on carbonaceous surfaces, *Phys. Chem. Chem. Phys.*, 1, 5443–5450, 1999.
- Knopf, D. A., Cosman, L. M., Mousavi, P., Mokamati, S., and Bertram, A. K.: A novel flow reactor for studying reactions on liquid surfaces coated by organic monolayers: Methods, validation, and initial results, *J. Phys. Chem. A*, 111, 11021–11032, 2007.
- Knopf, D. A., Mak, J., Gross, S., and Bertram, A. K.: Does atmospheric processing of saturated hydrocarbon surfaces by NO₃ lead to volatilization?, *Geophys. Res. Lett.*, 33, L17816, doi:10.1029/2006GL026884, 2006.
- Kuhn, M., Bultjes, P. J. H., Poppe, D., Simpson, D., Stockwell, W. R., Andersson-Skold, Y., Baart, A., Das, M., Fiedler, F., Hov, O., Kirchner, F., Makar, P. A., Milford, J. B., Roemer, M. G. M., Ruhnke, R., Strand, A., Vogel, B., and Vogel, H.: Intercomparison of the gas-phase chemistry in several chemistry and transport models, *Atmos. Environ.*, 32, 693–709, 1998.
- Letzel, T., Pöschl, U., Rosenberg, E., Grasserbauer, M., and Niessner, R.: In-source fragmentation of partially oxidized mono- and polycyclic aromatic hydrocarbons in atmospheric pressure chemical ionization mass spectrometry coupled to liquid chromatography, *Rapid Commun. Mass Sp.*, 13, 2456–2468, 1999a.
- Letzel, T., Rosenberg, E., Wissiack, R., Grasserbauer, M., and Niessner, R.: Separation and identification of polar degradation products of benzo[a]pyrene with ozone by atmospheric pressure chemical ionization-mass spectrometry after optimized column chromatographic clean-up, *J. Chromatogr. A*, 855, 501–514, 1999b.
- Letzel, T., Pöschl, U., Wissiack, R., Rosenberg, E., Grasserbauer, M., and Niessner, R.: Phenyl-modified reversed-phase liquid chromatography coupled to atmospheric pressure chemical ionization mass spectrometry: A universal method for the analysis of partially oxidized aromatic hydrocarbons, *Anal. Chem.*, 73, 1634–1645, doi:10.1021/ac001079t, 2001.

- Massman, W. J.: A review of the molecular diffusivities of H₂O, CO₂, CH₄, CO, O₃, SO₂, NH₃, N₂O, NO, and NO₂ in air, O₂ and N₂ near STP, *Atmos. Environ.*, 32, 1111–1127, 1998.
- Molina, M. J., Tso, T. L., Molina, L. T., and Wang, F. C. Y.: Antarctic Stratospheric Chemistry of Chlorine Nitrate, Hydrogen Chloride and Ice – Release of Active Chlorine, *Science*, 238, 1253–1257, 1987.
- Molina, M. J., Ivanov, A. V., T rakhtenberg, S. and Molina, L. T.: Atmospheric evolution of organic aerosol, *Geophys. Res. Lett.*, 31, L22104, doi:10.1029/2004GL020910, 2004.
- Nienow, A. M. and Roberts, J. T.: Heterogeneous chemistry of carbon aerosols, *Annu. Rev. Phys. Chem.*, 57, 105–128, doi:10.1146/annurev.physchem.57.032905.104525, 2006.
- Nishino, J.: Adsorption of water vapor and carbon dioxide at carboxylic functional groups on the surface of coal, *Fuel*, 80, 757–764, 2001.
- Osthoff, H. D., Roberts, J. M., Ravishankara, A. R., Williams, E. J., Lerner, B. M., Sommariva, R., Bates, T. S., Coffman, D., Quinn, P. K., Dibb, J. E., Stark, H., Burkholder, J. B., Talukdar, R. K., Meagher, J., Fehsenfeld, F. C., and Brown, S. S.: High levels of nitryl chloride in the polluted subtropical marine boundary layer, *Nat. Geosci.*, 1, 324–328, doi:10.1038/ngeo177, 2008.
- Park, J. H., Ivanov A. V., and Molina, M. J.: Effect of relative humidity on OH uptake by surfaces of atmospheric importance, *J. Phys. Chem. A*, 112, 6968–6977, 2008.
- Petters, M. D., Prenni, A. J., Kreidenweis, S. M., DeMott, P. J., Matsunaga, A., Lim, Y. B., and Ziemann, P. J.: Chemical aging and the hydrophobic-to-hydrophilic conversion of carbonaceous aerosol, *Geophys. Res. Lett.*, 33, 1107–1118, 2006.
- Popovicheva, O. B., Persiantseva, N. M., Tishkova, V., Shonija, N. K., and Zubareva, N. A.: Quantification of water uptake by soot particles, *Environ. Res. Lett.*, 3, 025009, doi:10.1088/1748-9326/3/2/025009, 2008.
- Pöschl, U.: Formation and decomposition of hazardous chemical components contained in atmospheric aerosol particles, *J. Aerosol Med.*, 15, 203–212, 2002.
- Pöschl, U.: Atmospheric aerosols: Composition, transformation, climate and health effects, *Angew. Chem., Int. Ed.*, 44, 7520–7540, doi:10.1002/anie.200501122, 2005.
- Pöschl, U., Letzel, T., Schauer, C., and Niessner, R.: Interaction of ozone and water vapor with spark discharge soot aerosol particles coated with benzo[a]pyrene: O₃ and H₂O adsorption, benzo[a]pyrene degradation, and atmospheric implications, *J. Phys. Chem. A*, 105, 4029–4041, 2001.
- Pöschl, U., Rudich, Y., and Ammann, M.: Kinetic model framework for aerosol and cloud surface chemistry and gas-particle interactions - Part 1: General equations, parameters, and terminology, *Atmos. Chem. Phys.*, 7, 5989–6023, 2007, <http://www.atmos-chem-phys.net/7/5989/2007/>.
- Rogaski, C. A., Golden, D. M., and Williams, L. R.: Reactive uptake and hydration experiments on amorphous carbon treated with NO₂, SO₂, O₃, HNO₃, and H₂SO₄, *Geophys. Res. Lett.*, 24, 381–384, 1997.
- Rogge, W. F., Mazurek, M. A., Hildemann, L. M., Cass, G. R., and Simoneit, B. R. T.: Quantification of urban organic aerosols at a molecular-level – identification, abundance and seasonal-variation, *Atmos. Environ. A-Gen.*, 27, 1309–1330, 1993.
- Rudich, Y.: Laboratory perspectives on the chemical transformations of organic matter in atmospheric particles, *Chem. Rev.*, 103, 5097–5124, doi:10.1021/cr020508f, 2003.
- Rudich, Y., Donahue, N. M., and Mentel, T. F.: Aging of organic aerosol: Bridging the gap between laboratory and field studies, *Annu. Rev. Phys. Chem.*, 58, 321–352, doi:10.1146/annurev.physchem.58.032806.104432, 2007.
- Saathoff, H., Naumann, K. H., Riemer, N., Kamm, S., Mohler, O., Schurath, U., Vogel, H., and Vogel, B.: The loss of NO₂, HNO₃, NO₃/N₂O₅, and HO₂/HOONO₂ on soot aerosol: A chamber and modeling study, *Geophys. Res. Lett.*, 28, 1957–1960, 2001.
- Schwartz, S. E.: NATO ASI Series, chapter: Mass-transport considerations pertinent to aqueous phase reactions of gases in liquid-water clouds, *Chemistry of Multiphase Atmospheric 15 Systems*, Springer, Berlin, Germany, G6, 415 pp., 1986.
- Schwartz, S. E. and Freiberg, J. E.: Mass-transport limitation to the rate of reaction of gases in liquid droplets – Application to oxidation of SO₂ in aqueous-solutions, *Atmos. Environ.*, 15, 1129–1144, 1981.
- Seinfeld, J. H. and Pandis, S.: *Atmospheric Chemistry and Physics: From Air Pollution to Climate Change*, Wiley-Interscience, New York, 2006.
- Seisel, S., Brensen, C., Vogt, R., and Zellner, R.: Kinetics and mechanism of the uptake of N₂O₅ on mineral dust at 298 K, *Atmos. Chem. Phys.*, 5, 3423–3432, 2005, <http://www.atmos-chem-phys.net/5/3423/2005/>.
- Shilling, J. E., King, S. M., Mochida, M., and Martin, S. T.: Mass spectral evidence that small changes in composition caused by oxidative aging processes alter aerosol CCN properties, *J. Phys. Chem. A*, 111, 3358–3368, doi:10.1021/jp068822r, 2007.
- Smith, D. M. and Chughtai, A. R.: Reaction kinetics of ozone at low concentrations with n-hexane soot, *J. Geophys. Res.-Atmos.*, 101, 19607–19620, 1996.
- Solomon, S., Mills, M., Heidt, L. E., Pollock, W. H., and Tuck, A. F.: On the evaluation of ozone depletion potentials, *J. Geophys. Res.-Atmos.*, 97, 825–842, 1992.
- Stemmler, K., Ammann, M., Donders, C., Kleffmann, J., and George, C.: Photosensitized reduction of nitrogen dioxide on humic acid as a source of nitrous acid, *Nature*, 440, 195–198, doi:10.1038/nature04603, 2006.
- Stephens, S., Rossi, M. J., and Golden, D. M.: The heterogeneous reaction of ozone on carbonaceous surfaces, *Int. J. Chem. Kinet.*, 18, 1133–1149, 1986.
- Stockwell, W. R., Middleton, P., Chang, J. S., and Tang, X. Y.: The 2nd generation regional acid deposition model chemical mechanism for regional air-quality modeling, *J. Geophys. Res.-Atmos.*, 95, 16343–16367, 1990.
- Stockwell, W. R., Kirchner, F., Kuhn, M., and Seefeld, S.: A new mechanism for regional atmospheric chemistry modeling, *J. Geophys. Res.-Atmos.*, 102, 25847–25879, 1997.
- Tabor, K., Gutzwiller, L., and Rossi, M. J.: Heterogeneous Chemical-Kinetics of NO₂ on Amorphous-Carbon at Ambient-Temperature, *J. Phys. Chem.*, 98, 6172–6186, 1994.
- Thomas, E. R., Frost, G. J., and Rudich, Y.: Reactive uptake of ozone by proxies for organic aerosols: Surface-bound and gas-phase products, *J. Geophys. Res.-Atmos.*, 106, 3045–3056, 2001.
- Tie, X., Brasseur, G., Emmons, L., Horowitz, L., and Kinnison, D.: Effects of aerosols on tropospheric oxidants: A global model study, *J. Geophys. Res.-Atmos.*, 106, 22931–22964, 2001.
- Tie, X., Madronich, S., Li, G. H., Ying, Z., Zhang, R., Garcia, A. R.,

- Lee-Taylor, J., and Liu, Y.: Characterizations of chemical oxidants in Mexico City: A regional chemical dynamical model (WRF-Chem) study, *Atmos. Environ.*, 41, 1989–2008, 2007.
- Van Gulijk, C., Marijnissen, J. C. M., Makkee, M., Mouljin, J. A., and Schmidt-Ott, A.: Measuring diesel soot with a scanning mobility particle sizer and an electrical low-pressure impactor: performance assessment with a model for fractal-like agglomerates, *J. Aerosol. Sci.*, 35, 633–655, doi:10.1016/j.jaerosci.2003.11.004, 2004.
- Vogel, B., Vogel, H., Kleffmann, J., and Kurtenbach, R.: Measured and simulated vertical profiles of nitrous acid – Part II, Model simulations and indications for a photolytic source, *Atmos. Environ.*, 37, 2957–2966, doi:10.1016/S1352-2310(03)00243-7, 2003.